Journal of
METAMORPHIC GEOLOGY

J. metamorphic Geol., 2013, **31,** 165–186 doi:10.1111/jmg.12008

Three steps of serpentinization in an eclogitized oceanic serpentinization front (Lanzo Massif – Western Alps)

B. DEBRET,[1,2,3] C. NICOLLET,[1,2,3] M. ANDREANI,[4] S. SCHWARTZ[5] AND M. GODARD[6]
[1]*Clermont Université, Université Blaise Pascal, Laboratoire Magmas et Volcans, Clermont-Ferrand, France (b.debret@opgc.univ-bpclermont.fr)*
[2]*CNRS, UMR6524, LMV, Clermont-Ferrand, France*
[3]*IRD, R163, LMV, Clermont-Ferrand, France*
[4]*Laboratoire de Géologie de Lyon, ENS – Université Lyon 1, Villeurbanne, France*
[5]*Institut des Sciences de la Terre, Université Grenoble I, Grenoble, France*
[6]*Géosciences Montpellier, Université Montpellier 2, Montpellier, France*

ABSTRACT The Lanzo peridotite massif is a fragment of oceanic lithosphere generated in an ocean–continent transition context and eclogitized during alpine collision. Despite the subduction history, the massif has preserved its sedimentary oceanic cover, suggesting that it may have preserved its oceanic structure. It is an exceptional case for studying the evolution of a fragment of the lithosphere from its oceanization to its subduction and then exhumation. We present a field and petrological study retracing the different serpentinization episodes and their impact on the massif structure. The Lanzo massif is composed of slightly serpentinized peridotites (< 20% serpentinization) surrounded by an envelope of foliated serpentinites (100% serpentinization) bordered by oceanic metabasalts and metasedimentary rocks. The limit between peridotites and serpentinites defines the front of serpentinization. This limit is sharp: it is marked by the presence of massive serpentinites (80% serpentinization) and, locally, by dykes of metagabbros and mylonitic gabbros. The deformation of these gabbros is contemporaneous with the emplacement of the magma. The presence of early lizardite in the peridotites testifies that serpentinization began during the oceanization, which is confirmed by the presence of meta-ophicarbonates bordering the foliated serpentinite envelope. Two additional generations of serpentine occur in the ultramafic rocks. The first is a prograde antigorite that partially replaced the lizardite and the relict primary minerals of the peridotite during subduction, indicating that serpentinization is an active process at the ridge and in the subduction zone. Locally, this episode is followed by the deserpentinization of antigorite at peak *P–T* (estimated in eclogitized metagabbros at 2–2.5 GPa and 550–620 °C): it is marked by the crystallization of secondary olivine associated with chlorite and/or antigorite and of clinopyroxene, amphibole and chlorite assemblages. A second antigorite formed during exhumation partially to completely obliterating previous textures in the massive and foliated serpentinites. Serpentinites are an important component of the oceanic lithosphere generated in slow to ultraslow spreading settings, and in these settings, there is a serpentinization gradient with depth in the upper mantle. The seismic Moho limit could correspond to a serpentinization front affecting the mantle. This partially serpentinized zone constitutes a less competent level where, during subduction and exhumation, deformation and fluid circulation are localized. In this zone, the reaction kinetics are increased and the later steps of serpentinization obliterate the evidence of this progressive zone of serpentinization. In the Lanzo massif, this zone fully recrystallized into serpentinite during alpine subduction and collision. Thus, the serpentinite envelope represents the oceanic crust as defined by geophysicists, and the sharp front of serpentinization corresponds to an eclogitized seismic palaeo-Moho.

Key words: antigorite; Lanzo; lizardite; Raman; serpentinization front.

INTRODUCTION

High-pressure (HP) serpentinites returned from former subduction zones and exposed in the Alps provide information on deep geochemical and geodynamical processes. Previous studies, based on geochemical and structural approaches, have proposed that serpentinites in ophiolites are relicts of a serpentinized channel, formed during an exhumation step and composed of a mélange between oceanic and mantle wedge serpentinites (Schwartz *et al.*, 2001; Guillot *et al.*, 2004; Deschamps *et al.*, 2011). However, recent investigations on ophiolites demonstrated the preservation of inherited ocean–continent transition (OCT) sedimentation (Beltrando *et al.*, 2010; Vitale-Brovarone *et al.*, 2011) questioning the origin of the Alpine serpentinites. The Lanzo massif is an exceptional case where peridotites are surrounded by eclogitized and exhumed serpentinite

envelope. Its study allows the reconstruction of the different serpentinization steps from oceanization to subduction and exhumation.

The Lanzo massif is composed of slightly serpentinized spinel/plagioclase peridotites and is surrounded by an envelope of foliated serpentinites of ~3–5 km thickness (Fig. 1; Boudier, 1978; Müntener *et al.*, 2005; Groppo & Compagnoni, 2007). Previous structural, petrographic and geochemical studies (Nicolas *et al.*, 1972; Piccardo *et al.*, 2007; Kaczmarek & Muntener, 2008, 2010) have shown that the oceanic exhumation of the Lanzo massif occurred in an OCT context. U-Pb zircon dating of magmatic intrusions in Lanzo peridotites gives an age of 163.5 Ma (Rubatto *et al.*, 2008), contemporaneous with massif oceanic exhumation. The Lanzo peridotites have a fertile composition with respect to primitive mantle abundance (Piccardo *et al.*, 2007), and the rare gabbro and dolerite dykes cross-cutting the ultramafic rocks show MORB composition (Bodinier *et al.*, 1986; Bodinier, 1988). This suggests that the Lanzo massif is a portion of oceanic lithosphere generated in a magma-poor setting. In this context, the exposure of mantle peridotite on the ocean floor is common, as observed along slow and ultraslow spreading ridges (Cannat *et al.*, 1995; Dick *et al.*, 2003; Mével, 2003). Thus, the upper part of the oceanic lithosphere is mainly made up of serpentinites, and the Moho discontinuity, such as defined by seismic speeds of Vp = 8 km s^{-1}, cannot correspond to a petrological transition between mantle and a magmatic crust, but fits better with a serpentinization front affecting the mantle (Canales *et al.*, 2000; Mével, 2003).

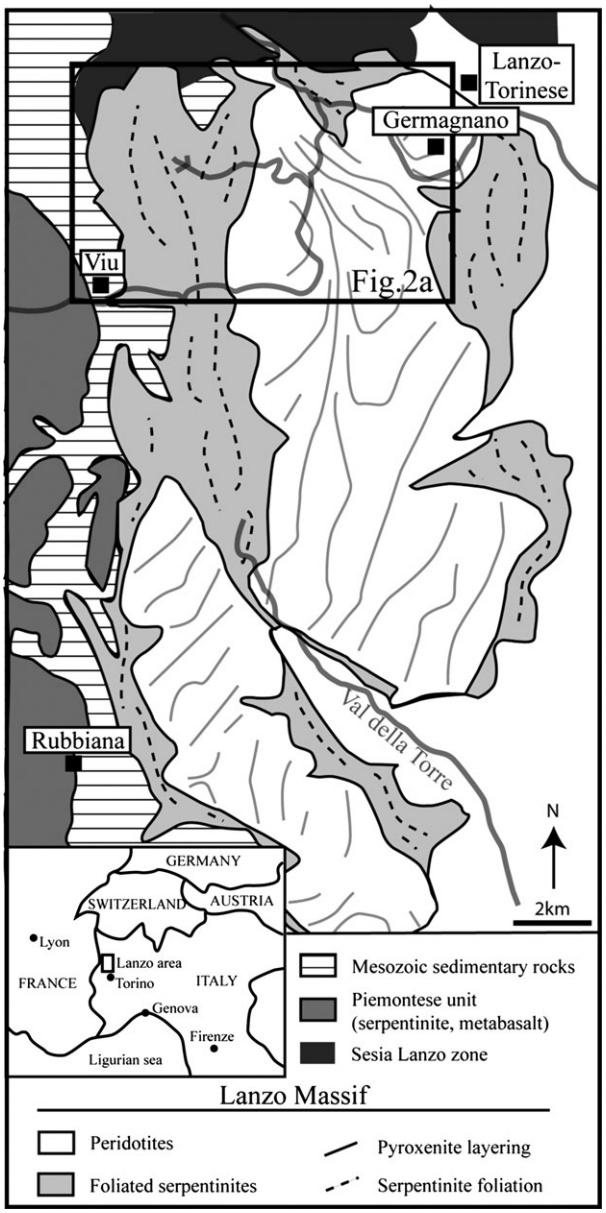

Fig. 1. Geological map of Lanzo massif and its environment (modified after Boudier, 1978). The box corresponds to the studied area illustrated in Fig. 2.

The Lanzo massif also records HP Alpine subduction metamorphism between 55 and 46.5 Ma (Rubatto *et al.*, 2008). Despite its subduction history, the massif largely preserves its oceanic structure. In the northwest of the massif, a serpentinite envelope is bounded by a metasedimentary cover of ophicarbonates, Mn-rich metaquartzites and metabasites (Lagabrielle *et al.*, 1989; Pelletier & Müntener, 2006). These rocks result from oceanic sedimentation during the exposure of the lithospheric mantle of the Lanzo on the oceanic floor. Pelletier & Müntener (2006) have shown that these metasedimentary rocks record the same evolution as the ultramafic body of the Lanzo during the Alpine subduction. As proposed in the Zermatt zone, this strongly suggests that this lithostratigraphic association, consisting of post-rift sedimentary rocks above ultramafic rocks, was preserved during the subduction (Beltrando *et al.*, 2010).

To clarify the origin of the contact between the serpentinite envelope and the slightly serpentinized peridotites, we unraveled the different serpentinization episodes and their impact on the massif structure. The different serpentine polymorphs were identified by coupling petrographic study, microprobe analysis and Raman spectroscopy. The microstructural relationships between the different serpentine generations allow us to propose a qualitative *P–T* evolution of ultramafic rocks and their serpentinization history while studying the gabbros permits us to quantify the *P–T* path. From these results, a structural evolution of the lithospheric mantle is proposed from its oceanic floor alteration to its subduction metamorphism and retrograde evolution during Alpine collision.

STUDIED AREA

The Lanzo massif is an eclogitized ultramafic body of 150 km^2, located 30 km to the northwest of Turin (Italy) in the western Alps. It is bounded by the sediments of Po plain to the east and south, by meta-ophiolites and the

Schistes Lustrés unit in the west and by the HP metamorphic continental unit of Sesia in the north. Previous studies (Nicolas *et al.*, 1972; Bodinier, 1988; Kaczmarek & Muntener, 2008) divided the Lanzo massif into three parts separated by two partially serpentinized mylonitic shear zones formed during its oceanic exhumation in an OCT context. The entire massif is composed of a central part of slightly serpentinized lherzolites (0–20% of serpentine) surrounded by 3–5 km thick envelope of foliated serpentinites (~100% of serpentine), with sometimes, a thin intermediate zone (< 150 m) of massive serpentinites (~80% of serpentine). Oceanic ophicarbonate rocks locally compose the external part of foliated serpentinite envelope (Lagabrielle *et al.*, 1989; Pelletier & Müntener, 2006; Kaczmarek & Muntener, 2008). They occur as highly brecciated rocks built up of serpentinite fragments with an irregular interlayered carbonate matrix. Detailed mapping of the lithologies bordering the serpentinite envelope revealed the presence of a thin sequence of metamorphosed oceanic metasedimentary rocks and MORB-type volcanic rocks associated with metaophicarbonate (Lagabrielle *et al.*, 1989; Pelletier & Müntener, 2006). This suggests that the Lanzo ultramafic massif preserved its oceanic cover.

The study is focused on the northern part of the massif (Fig. 2a) where the connection between the metasedimentary cover and the ultramafic rocks has been established (Lagabrielle *et al.*, 1989; Pelletier & Müntener, 2006). Results are presented from the Toglie and Germagnano areas (Fig. 2) where there are cross-sections from slightly serpentinized peridotites, massive serpentinite to foliated serpentinite.

The Toglie cross-section to the southwest is ~4 km long (Fig. 2), with the western part of the composed of

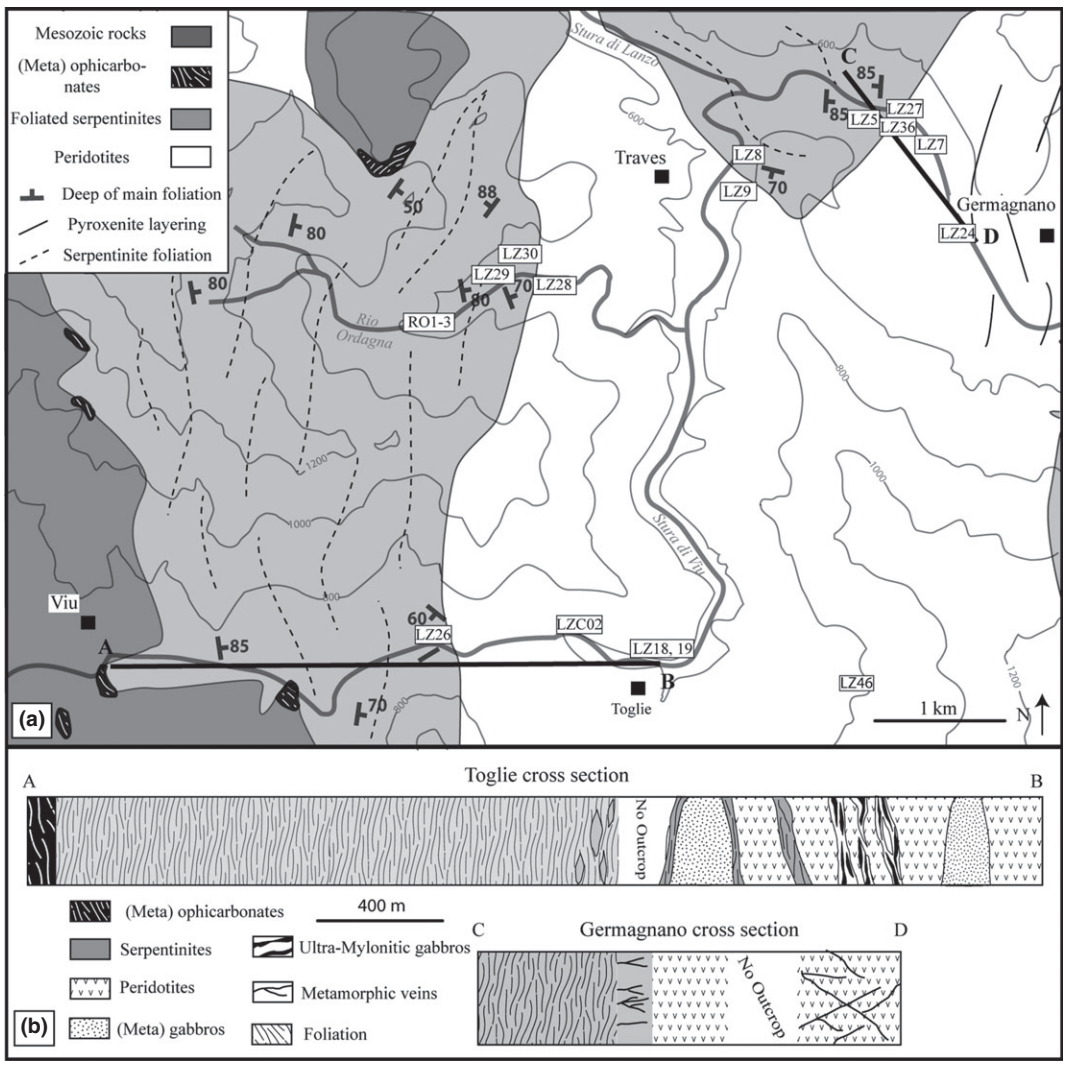

Fig. 2. (a) Geological map of the studied area of Lanzo massif. LZXX: sample localization. (b) Two studied synthetic cross-sections of Toglie and Germagnano. In the Toglie cross-section, the structure of the serpentinization front is partially dismantled: the deformation affects the massive serpentinite zone, and the vegetation has covered the contact between serpentinite and peridotites. In the Germagnano cross-section, the serpentinization front is preserved from the deformation, but the sedimentary cover has not been observed.

foliated serpentinites. Just above the peridotite/serpentinite contact, the serpentinite foliation envelops metric lenses of massive serpentinites. The contact between these serpentinites and the slightly serpentinized peridotites does not outcrop. Nevertheless, the serpentinization front is sharp, passing from serpentinite to peridotites over few decametres. Towards the east, a 50 m long area of serpentinized peridotites is crossed by decimetric dykes of mylonitic metagabbros. Those are sometimes connected to metric to decimetric pods of metagabbros intersected by dykes of metadolerites.

The Germagnano cross-section lies to the north (Fig. 2b), along which there are three ultramafic lithologies, foliated serpentinites, massive serpentinites and slightly serpentinized peridotites. The limit between massive serpentinites and peridotites is sharp and delimits the front of serpentinization.

PETROGRAPHY, FIELD RELATIONSHIPS AND THERMOBAROMETRY

Method

The characterization of the different serpentine generations was determined by coupling petrographic study with microprobe analysis and Raman spectroscopy. This latter analytical method is commonly used to discriminate serpentine structural type (Rinaudo *et al.*, 2003; Auzende *et al.*, 2006; Groppo *et al.*, 2006).

Raman spectroscopy was performed at the Laboratoire des Sciences de la Terre of the ENS-Lyon, in France, using a LabRam HR800 Raman microspectrometer. A light source (wavelength = 514 nm, power = 700 μW, resolution = 600 g mm^{-1}) was coupled to an OlympusTM BX30 open microscope equipped with an ×100 objective to focus the laser beam into 1 m spot diameter. The backscattered Raman signal was collected with the same objective. Acquisition time was between 5 and 30 s. On each spectra, a base line was fixed using the PeakFit© software. The spectral regions from 150 to 1300 cm^{-1} and from 3500 to 3900 cm^{-1} were investigated. According to literature data (Rinaudo *et al.*, 2003; Groppo *et al.*, 2006), those frequency regions can differentiate lizardite from antigorite. In the low-frequency region, the lizardite can be clearly identified with a weak broad peak ~1080 cm^{-1}, while the antigorite presents an sharp peak ~1043 cm^{-1}. OH stretching modes are observed between 3500 and 3750 cm^{-1}. They are characterized in lizardite by two broad peaks near 3670 and 3697 cm^{-1}, and by two principal peaks near 3685 and 3703 cm^{-1} in antigorite (Rinaudo *et al.*, 2003; Auzende *et al.*, 2004).

In situ major element analyses of minerals of ultramafic rocks have been performed with a microprobe CAMECA SX 100 at the Laboratoire Magmas et Volcans in Clermont Ferrand (France). For ultramafic rocks, four samples of slightly serpentinized peridotites, four samples of massive serpentinites and one sample of foliated serpentinite were analysed. For metabasites, two samples of mylonitic metagabbros and two metagabbro pods were analysed.

Serpentine minerals have been characterized and compositional variation established by focusing on Fe, Al and Cr (Dungan, 1979; Viti & Mellini, 1998; Andreani *et al.*, 2007). Primary mantle olivine has been distinguished from metamorphic olivine using X_{Mg} ratio (= Mg/(Fe + Mg)), and the variations in NiO and MnO contents (Trommsdorff *et al.*, 1998; Scambelluri *et al.*, 1991; Nozaka, 2003), metamorphic olivine having classically a lower X_{Mg} and a higher MnO content than mantle olivine. For pyroxene, Nozaka (2010) proposed that metamorphic clinopyroxene is systematically depleted in Cr_2O_3 and Al_2O_3 compared with primary pyroxene, despite their compositional variation due to original rock composition.

Ultramafic rocks

Slightly serpentinized peridotites

Peridotites of the Lanzo massif are mostly spinel- and plagioclase-bearing lherzolites and have a primary magmatic layering marked by clinopyroxenite layers (Fig. 2a). They are composed of olivine, brown orthopyroxene and green clinopyroxene in relief on the outcrop surface (grain size between 1 mm and ~1 cm) and pluri-millimetric black spinel grains surrounded by white corona of chlorite and tremolite. In most of the ultramafic rocks, plagioclase is replaced during the alpine metamorphism by HP aggregates of zoisite, jadeite and garnet micro-crystals. However, fresh plagioclase has been locally observed surrounding spinel (Fig. 3a) and forming veinlets that have been interpreted as products of the incipient crystallization of percolating melts (Piccardo *et al.*, 2007).

In slightly serpentinized peridotites, the major element composition of primary minerals is similar to those reported in the literature (Piccardo *et al.*, 2007). The X_{Mg} of olivine is 0.86–0.90; the NiO and MnO are between 0.26–0.40 and 0.09–0.25 wt%, respectively (Fig. 4a). The X_{Mg} of clinopyroxene varies from 0.90 to 0.94 in the slightly serpentinized peridotites, and Al_2O_3 (2.90–5.54 wt%) and Cr_2O_3 (1.00–1.54 wt%) contents are high (Fig. 4b). Olivine is surrounded and crossed by serpentine veins, which represent the first step of serpentinization of peridotites, when hydration is limited (Viti & Mellini, 1998). Two generations of veins were distinguished.

The first generation (V1) has a regular shape, with width ranging from a few to several hundred micrometres (Fig. 3b–d). They consist of parallel, fine elongate grains, slightly orange under plane polarized light and displaying an undulatory extinction, perpendicular to footwalls in crossed-polarized light. Magnetite is present within the vein centre as a fine line of micrometric grain aggregates. These veins also crosscut orthopyroxene and replace orthopyroxene exsolutions

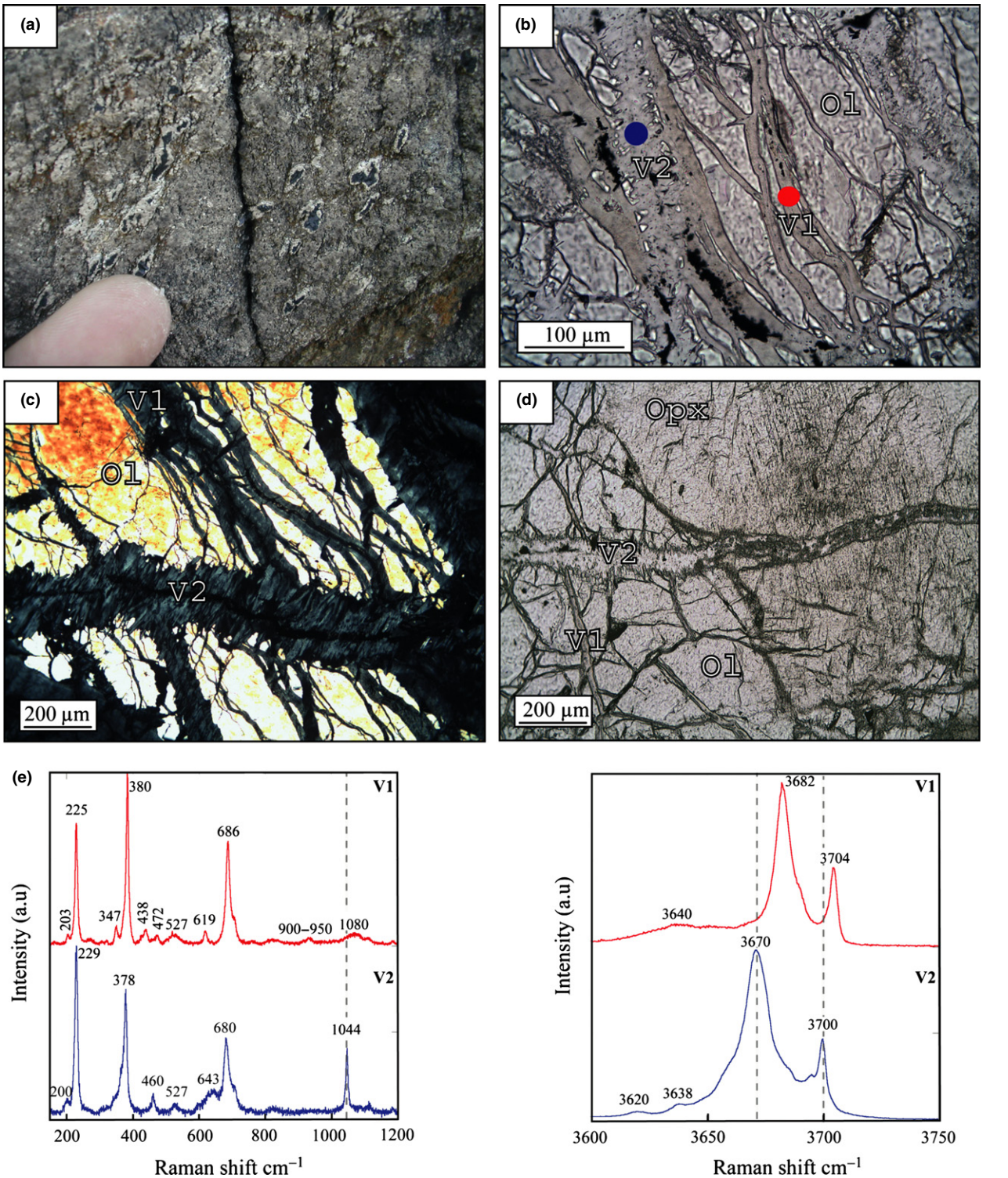

Fig. 3. (a) Peridotite of Monte Magdalena showing plagioclase coronas surrounding spinel. (b–d) Microphotographs of a slightly serpentinized peridotite of Toglie cross-section (LZC02). (b) Microphotograph (plane polarized light) of an antigorite vein (V2) crossing lizardite vein (V1) and olivine. Note that a fine string of magnetite is present in the centre of V1; V2 boundaries contain minute secondary olivine grains. V2 grows on V1. Mineral abbreviations are from Whitney & Evans (2010). (c) Microphotograph (cross polarized light) of V2 crossing V1. (d) Microphotograph (plane polarized light) of an antigorite vein crossing an olivine and an orthopyroxene. When it crosses the orthopyroxene, the vein centre is made of tremolite and clinopyroxene granulas. (e) Raman spectra of lizardite (V1) and antigorite (V2). Corresponding Raman spots are indicated on (b) (red and blue points). Dotted lines indicate the discriminating peaks of antigorite spectra and lizardite spectra.

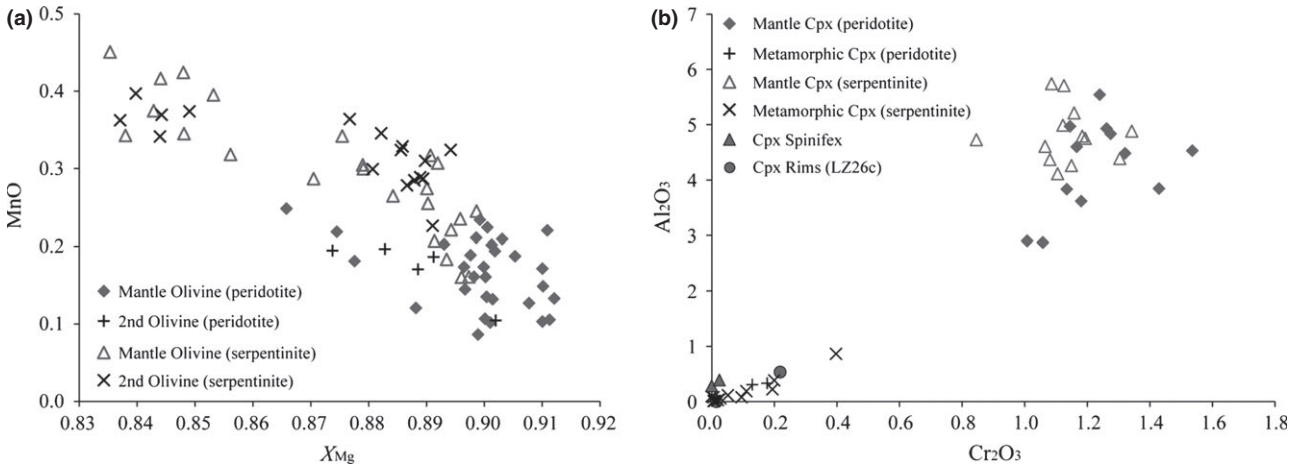

Fig. 4. (a) MnO (wt%) *v.* X_{Mg} contents of primary mantle olivine and secondary olivine (Ol_2) in slightly serpentinized peridotites and serpentinites. (b) Al_2O_3 (wt%) *v.* Cr_2O_3 (wt%) contents of primary clinopyroxene and metamorphic clinopyroxene in slightly serpentinized peridotites and serpentinites.

in the clinopyroxene. Raman spectra of serpentine V1 (Fig. 3e) are similar to lizardite spectra reported in literature (Rinaudo *et al.*, 2003; Auzende *et al.*, 2004). In addition, further modulations of the spectrum could be attributable to cation substitutions. In fact, the lizardite veins display a large range of FeO (3.90–8.25 wt%) and Al_2O_3 (0.01–4.90 wt%) contents. High Al_2O_3 + FeO (3.90–9.85 wt%) content have to be accommodated by high Al or Fe substitutions for Mg and/or Si. Thus, the unusual broad band at 3650 cm^{-1} could be assigned to stretching of OH bonded to octahedral site linked to Si-Al/Fe substitutions (Mellini, 1982; Prietto *et al.*, 1991). Similarly, the shift of the 388 cm^{-1} vibration mode to 380 cm^{-1} could correspond to Al or Fe substitution for Si (Groppo *et al.*, 2006) and the large band in the 900–950 cm^{-1} spectral region could be attributed to Al or Fe substitution for Mg in octahedral layers (Groppo *et al.*, 2006).

Veins2 (V2) show an irregular shape with width up to 100 μm (Fig. 3b,c). They consist of more or less parallel coarse flakes nearly perpendicular to the vein selvage. Magnetite is present as isolated micrometric grains within the vein centre. Veins2 grow at the expense of lizardite veins (Fig. 3b) and also at the expense of primary minerals, olivine, orthopyroxene, orthopyroxene exsolutions in clinopyroxene and sometimes clinopyroxene. Raman spectra of serpentine V2 (Fig. 3e) are identical to antigorite spectra reported in literature (Rinaudo *et al.*, 2003; Auzende *et al.*, 2004).

The lizardite (V1) and antigorite (V2) veins retain the chemical signature of their precursor. Serpentine veins crosscutting pyroxene have higher Al and Cr contents than serpentine veins crosscutting olivine (Table 1). Despite their relative similarity, several differences between antigorite and lizardite chemical analyses were noted. As with the data of Dungan (1979), antigorite has lower H_2O content (estimated by difference to 100) and relative high SiO_2 compared with lizardite (Table 2). Thus, the antigorite that grew at the expense of lizardite implies a release of H_2O: lizardite $\Rightarrow$ antigorite + H_2O.

Where antigorite veins crosscut orthopyroxene, they have a banded texture (Fig. 3d) with the centre composed of granoblastic aggregates of clinopyroxene and tremolite, and the boundaries of antigorite. This unusual texture suggests that clinopyroxene and tremolite assemblages were formed from antigorite. The clinopyroxene granoblasts have higher X_{Mg} (~0.96) and lower Al_2O_3 (< 0.34 wt%) and Cr_2O_3 (< 0.18 wt%) contents than mantle clinopyroxene (Table 1, Fig. 4b).

Locally, the antigorite veins crossing olivine show similar textures (Fig. 5a), with the centre composed of minute granoblastic olivine (< 10 μm). This texture suggests that this olivine is formed at the expense of the antigorite. Raman spectra of primary olivine are similar to a forsterite reference spectrum from the RRUFF database (ID: R040018). However, secondary olivine presents an unusual spectrum with additional antigorite peaks (Fig. 5b). The secondary olivine has similar NiO (0.25–0.34 wt%), MnO (0.10–0.19 wt%) and X_{Mg} (0.87–0.88) to mantle olivine (Fig. 4a).

At the Toglie cross-section, the slightly serpentinized peridotites are divided by a network of serpentinized channels, with a width up to 2 mm, where olivine and orthopyroxene are completely replaced by mesh and bastite textures. Mesh textures consist of a grey homogenous area of serpentine with undulatory extinction delimited by fibrous rims. Bastite textures consist of white serpentine grains elongated parallel to the original cleavages of the pyroxene. These textures are typical of oceanic lizardite (Boudier, 1971; Wicks & Whittaker, 1977) and are crossed by antigorite veins. They represent relicts of early fluid circulation channels (Viti & Mellini, 1998; Andreani *et al.*, 2007). The Raman spectra and the major

Table 1. Microprobe analysis of peridotite and serpentinite minerals. Cations are normalized to seven oxygen for serpentine, four oxygen for olivine, six oxygen for clinopyroxene and 28 oxygen for chlorite.

	Peridotite												Massive Serpentinite								Foliated serpentinite	
Sample	LZ24		LZC02							LZ19		LZ35b	LZ34c						LZ34b		RO3	
Mineral Previous	Liz Opx	Liz Opx	Liz Ol	Liz Ol	Atg Opx	Atg Opx	Atg Ol	Cpx	Cpx2 Atg	Ol	Ol2 Atg	Chl Sp	Atg1 Px	Atg2 Px	Atg1 Ol	Atg2 Ol	Chl Sp	Chl	Ol2 Atg	Chl	Atg2 Px	Atg2 Ol
SiO_2	36.31	39.70	40.91	43.08	44.14	41.27	43.31	50.80	55.58	40.95	40.62	29.37	40.04	43.05	43.15	43.43	29.30	34.52	40.99	35.77	42.92	43.56
TiO_2	0.00	0.13	0.04	0.00	0.00	0.00	0.00	0.61	0.02	0.01	0.00	0.08	0.00	0.04	0.01	0.00	0.02	0.06	0.03	0.00	0.01	0.00
Al_2O_3	8.87	4.90	0.01	0.10	1.68	3.47	0.18	5.54	0.03	0.01	0.07	22.45	5.99	1.45	2.44	1.72	22.37	13.91	0.00	10.42	1.58	1.26
FeO	2.92	7.17	3.90	1.84	3.31	7.28	3.37	2.82	1.28	12.06	11.89	2.92	3.42	3.23	3.41	3.38	3.66	3.51	10.58	3.32	4.68	4.46
NiO	0.17	0.21	0.29	0.06	0.09	0.07	0.10	0.04	0.00	0.34	0.34	0.17	0.23	0.10	0.18	0.15	0.19	0.22	0.32	0.21	0.05	0.08
MnO	0.01	0.30	0.05	0.05	0.03	0.04	0.02	0.07	0.11	0.22	0.19	0.02	0.02	0.02	0.01	0.04	0.05	0.01	0.31	0.02	0.06	0.11
MgO	32.90	29.71	41.40	41.57	37.89	33.11	39.51	15.14	18.74	47.13	46.16	30.39	37.08	38.34	37.20	38.17	30.44	32.96	47.89	35.24	37.16	36.94
CaO	0.74	0.31	0.03	0.03	0.73	0.14	0.01	23.32	24.22	0.00	0.02	0.01	0.01	0.02	0.05	0.00	0.02	0.09	0.01	0.03	0.12	0.04
Na_2O	0.38	0.19	0.03	0.01	0.04	0.05	0.08	0.44	0.08	0.00	0.00	0.01	0.00	0.08	0.00	0.01	0.04	0.05	0.02	0.03	0.30	0.18
K_2O	0.08	0.15	0.03	0.03	0.01	0.41	0.04	0.02	0.04			0.03	0.07	0.08	0.01	0.00	0.02	0.04		0.00	0.05	0.06
Cr_2O_3	2.36	2.31	0.01	0.01	0.31	0.93	0.02	1.24	0.01	0.01	0.00	0.24	0.69	0.53	0.00	0.02	0.00	1.31	0.00	0.04	0.20	0.04
Total	84.74	85.07	86.69	86.77	88.24	86.79	86.64	100.05	100.11	100.71	99.29	85.69	87.56	86.94	86.46	86.93	86.09	86.69	100.15	85.09	87.14	86.72
H_2O[a]	15.26	14.93	13.3	13.2	11.8	13.2	13.4					14.31	12.44	13.06	13.54	13.07	13.91	13.31		14.91	12.9	13.3
Si	1.77	1.95	1.94	2.01	2.04	1.98	2.04	1.86	2.00	1.01	1.01	5.60	1.87	2.02	2.02	2.03	5.59	6.54	1.01	6.88	2.02	2.05
Al	0.51	0.28	0.00	0.01	0.09	0.20	0.01	0.24	0.00	0.00	0.00	5.05	0.33	0.08	0.14	0.09	5.03	3.11	0.00	2.36	0.09	0.07
Ti	0.00	0.00	0.00	0.00	0.00	0.00	0.00	0.02	0.00	0.00	0.00	0.01	0.00	0.00	0.00	0.00	0.00	0.01	0.00	0.00	0.00	0.00
Fe	0.12	0.29	0.15	0.07	0.13	0.29	0.13	0.09	0.04	0.25	0.25	0.47	0.13	0.13	0.13	0.13	0.58	0.56	0.22	0.53	0.18	0.18
Ni	0.01	0.01	0.01	0.00	0.00	0.00	0.00	0.00	0.00	0.01	0.01	0.03	0.01	0.00	0.01	0.01	0.03	0.03	0.01	0.03	0.00	0.00
Mg	2.39	2.18	2.93	2.89	2.60	2.37	2.77	0.82	1.01	1.73	1.71	8.64	2.58	2.68	2.60	2.66	8.65	9.31	1.75	10.11	2.61	2.59
Mn	0.00	0.01	0.00	0.00	0.00	0.00	0.00	0.00	0.00	0.00	0.00	0.00	0.00	0.00	0.00	0.00	0.01	0.00	0.01	0.00	0.00	0.00
Na	0.04	0.02	0.00	0.00	0.00	0.00	0.01	0.03	0.01	0.00	0.00	0.01	0.00	0.01	0.00	0.00	0.01	0.02	0.00	0.01	0.03	0.02
Ca	0.04	0.02	0.00	0.00	0.04	0.01	0.00	0.91	0.94	0.00	0.00	0.00	0.00	0.00	0.00	0.00	0.00	0.02	0.00	0.01	0.01	0.00
K	0.00	0.01	0.00	0.00	0.00	0.03	0.00	0.00	0.00			0.01	0.00	0.00	0.00	0.00	0.01	0.01		0.00	0.00	0.00
OH	4.00	4.00	4.00	4.00	4.00	4.00	4.00					16.00	4.00	4.00	4.00	4.00	16.00	16.00		0.01	4.00	4.00
Cr	0.09	0.09	0.00	0.00	0.01	0.04	0.00	0.04	0.00	0.00	0.00	0.04	0.03	0.02	0.00	0.00	0.00	0.20	0.00	16.00	0.01	0.00
Total	8.96	8.87	9.06	8.99	8.92	8.92	8.96	4.01	4.00	2.99	2.99	35.85	8.95	8.94	8.91	8.92	35.91	35.81	2.99	35.94	8.95	8.92

[a]Estimated by difference.

Table 2. Microprobe analysis of amphibole of mylonitic gabbros. Cations are normalized to 23 oxygen. Results of Ernst & Liu (1998) thermometer are reported in °C.

	Hornblende porphyroclasts			Hornblende blebs			Hornblende granoblasts				Replacive hornblende				
SiO_2	43.19	43.73	44.06	43.31	43.18	42.62	42.97	42.93	43.06	43.47	45.05	46.01	45.90	43.10	43.96
TiO_2	5.25	5.02	5.05	4.57	4.60	4.69	3.79	3.85	4.26	4.31	3.08	1.12	1.09	0.66	0.37
Al_2O_3	10.57	10.50	10.04	10.57	10.19	10.59	10.97	11.17	11.06	10.65	8.67	8.43	8.40	11.55	11.41
FeO	10.11	10.22	10.08	10.07	10.31	11.15	10.72	10.68	10.41	10.19	12.89	13.50	13.52	16.20	13.77
MnO	0.08	0.18	0.25	0.22	0.18	0.22	0.13	0.17	0.15	0.24	0.34	0.26	0.30	0.07	0.11
MgO	14.26	13.76	13.81	13.79	13.97	13.34	13.46	13.78	13.66	13.85	13.74	14.02	14.08	10.91	13.35
CaO	10.34	10.65	10.26	11.27	11.30	10.77	11.71	11.43	11.34	11.56	10.19	10.86	11.03	10.75	9.87
Na_2O	3.57	3.81	3.81	3.40	3.33	3.28	3.19	2.91	3.02	3.13	4.09	3.46	2.99	3.97	3.92
K_2O	0.19	0.17	0.15	0.15	0.11	0.41	0.16	0.22	0.32	0.27	0.24	0.25	0.24	0.15	0.26
Cr_2O_3	0.11	0.13	0.57	0.08	0.04	0.08	0.06	0.05	0.08	0.12	0.00	0.00	0.00	0.02	0.02
Total	97.67	98.16	98.08	97.44	97.22	97.15	97.17	97.19	97.36	97.78	98.30	97.91	97.57	97.37	97.02
Si	6.30	6.36	6.41	6.35	6.35	6.30	6.34	6.32	6.32	6.35	6.61	6.77	6.78	6.48	6.53
Ti	0.58	0.55	0.55	1.83	1.77	1.85	1.91	1.94	1.91	1.83	0.34	0.12	0.12	0.07	0.04
Al	1.82	1.80	1.72	0.50	0.51	0.52	0.42	0.43	0.47	0.47	1.50	1.46	1.46	2.04	2.00
Fe	1.23	1.24	1.23	1.23	1.27	1.38	1.32	1.31	1.28	1.25	1.58	1.66	1.67	2.04	1.71
Mn	0.01	0.02	0.03	0.03	0.02	0.03	0.02	0.02	0.02	0.03	0.04	0.03	0.04	0.01	0.01
Mg	3.10	2.98	2.99	3.01	3.06	2.94	2.96	3.02	2.99	3.02	3.01	3.08	3.10	2.44	2.96
Ca	1.01	1.07	1.07	0.97	0.95	0.94	0.91	0.83	0.86	0.89	1.16	0.99	0.86	1.16	1.13
Na	1.62	1.66	1.60	1.77	1.78	1.71	1.85	1.80	1.78	1.81	1.60	1.71	1.75	1.73	1.57
K	0.04	0.03	0.03	0.03	0.02	0.08	0.03	0.04	0.06	0.05	0.04	0.05	0.04	0.03	0.05
Cr	0.01	0.01	0.07	0.01	0.00	0.01	0.01	0.01	0.01	0.01	0.00	0.00	0.00	0.00	0.00
OH				2.00	2.00	2.00	2.00	2.00	2.00	2.00	2.00	2.00	2.00	2.00	2.00
Total	15.72	15.73	15.70	17.73	17.74	17.76	17.76	17.72	17.71	17.72	17.90	17.88	17.82	18.00	17.99
T (°C)	1030	1032	1032	1028	1028	1030	1000	1003	1020	1022	951	700	696	616	559

element content of mesh and bastite textures are similar to lizardite veins.

To the south of the Germagnano cross-section, peridotites are crossed by a parallel vein network with a centimetric width and appearing in relief on outcrop surface (Fig. 6a). The vein is orange with a white centre, a few millimetres thick, in relief composed of homogeneous antigorite areas (confirmed by Raman spectroscopy, atg1), crossed by fractures in which secondary olivine grew (Fig. 6b). The Raman spectra

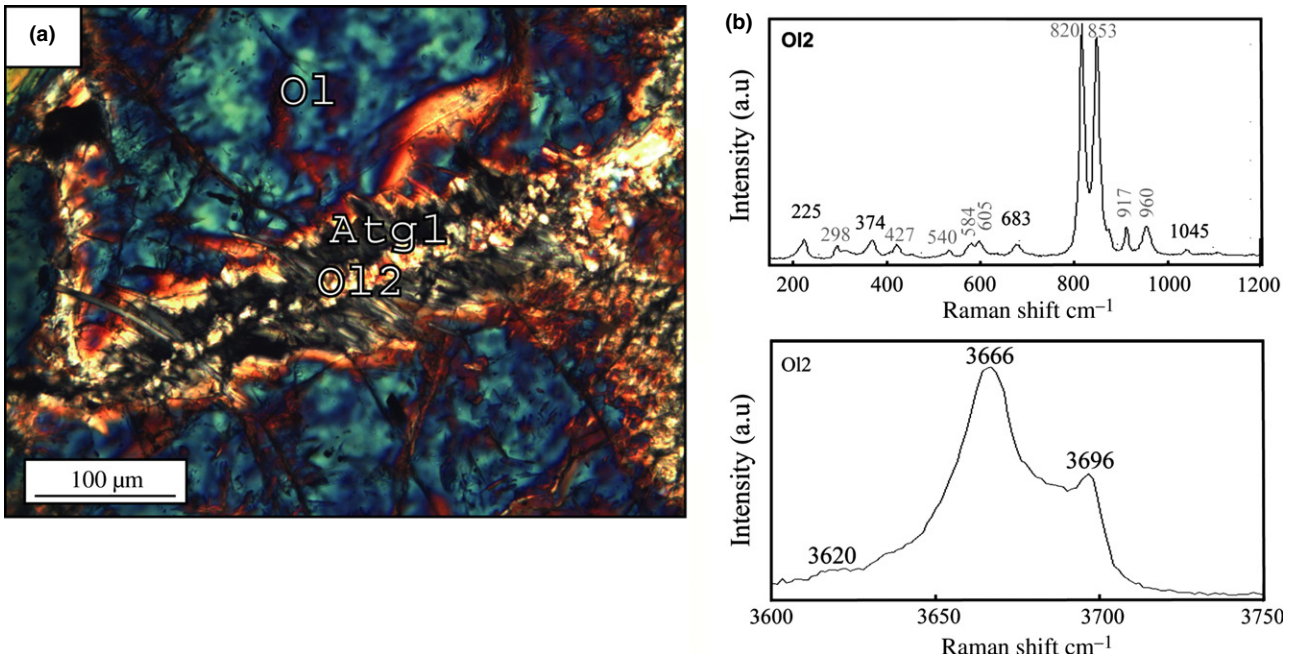

Fig. 5. (a) Microphotograph (cross polarized light) of an antigorite vein crossing an olivine with granoblastic secondary olivine (Ol2) at its centre. (b) Raman spectra of the granoblastic olivine. The secondary olivine possesses additional peaks (black values) corresponding to antigorite (usual peak values of olivine are in grey).

of this secondary olivine present additional lizardite peaks similar to those described previously (Fig. 5b). The orange part of the veins is several centimetres wide and composed of minute olivine of ~10 μm (Fig. 6c). Corresponding olivine Raman spectra are similar to primary mantle olivine spectra suggesting that they correspond to primary recrystallized olivine. The composition of secondary olivine (NiO = no data available, MnO = 0.19–0.20 wt% and X_{Mg} = 0.88–0.89) is similar to primary recrystallized olivine and mantle olivine (NiO = 0.30–0.48 wt%, MnO = 0.10–0.23 wt%, X_{Mg} = 0.90–0.91, Fig. 4a). A second generation of non-oriented antigorite lamellae (atg2) has grown on secondary olivine, primary minerals and atg1 (Fig. 6c). Chlorite areas of several millimetres crystallize on primary recrystallized olivine. Those areas contain spinifex clinopyroxene partially amphibolitized in actinolite (Fig. 6d). The Al_2O_3 (0.08–0.39 wt%) and Cr_2O_3 (0–0.01 wt%) contents and X_{Mg} (0.90–0.93) of the spinifex clinopyroxene differ from mantle clinopyroxene (Fig. 4b).

The peridotite/serpentinite contact of the Toglie cross-section

The peridotite/serpentinite contact is marked by metric to decametric lenses of massive serpentinite surrounded by the foliation of foliated serpentinites. They are mainly made of a dark grey serpentine matrix containing black or white millimetric crystals of peridotitic protolith (olivine < 5%, clinopyroxene < 5% and spinel < 1%).

Among the peridotite minerals, the clinopyroxene and spinel are the least affected by the serpentinization. Clinopyroxene can be totally preserved while orthopyroxene has disappeared, even where it exsolved in the clinopyroxene. In most cases, however, the clinopyroxene is partially replaced by serpentine lamellae oriented parallel to its cleavages. Its composition is zoned: the clinopyroxene core (Al_2O_3 = 4.11–5.21 wt%, Cr_2O_3 = 0.85–1.34 wt%, X_{Mg} = 0.91–0.92) has similar composition to that of slightly serpentinized peridotite while its rim has a low Al_2O_3 (0.00–0.53 wt%) and Cr_2O_3 (0.02–0.22 wt%, Fig. 4b) contents and a high X_{Mg} (0.97–0.98). Spinel is surrounded by a thin chlorite and, sometimes, tremolite corona. Rare olivine relicts have a low NiO content (0.00–0.03 wt%) and X_{Mg} (0.77–0.87) and a high MnO content (0.75–1.8 wt%) suggesting that their composition (and maybe the clinopyroxene rims) was highly modified by chemical interaction with MORB-type melts (e.g., Drouin *et al.*, 2009).

The matrix of the massive serpentinite is composed of large homogenous grey areas of several millimetres with a dirty appearance (atg1, Fig. 7a), a weak birefringence and sometimes an undulatory extinction. Corresponding Raman spectra are intermediate between lizardite and antigorite (Fig. 7b). In a low-frequency region, they are characterized by an intense peak ~1043 cm^{-1} (antigorite) and a weak broad peak ~1080 cm^{-1} (lizardite). In high-frequency region, the spectra present two intense peaks at 3673 and 3700 cm^{-1} corresponding to antigorite and a weak peak at 3685 cm^{-1} corresponding to lizardite. We

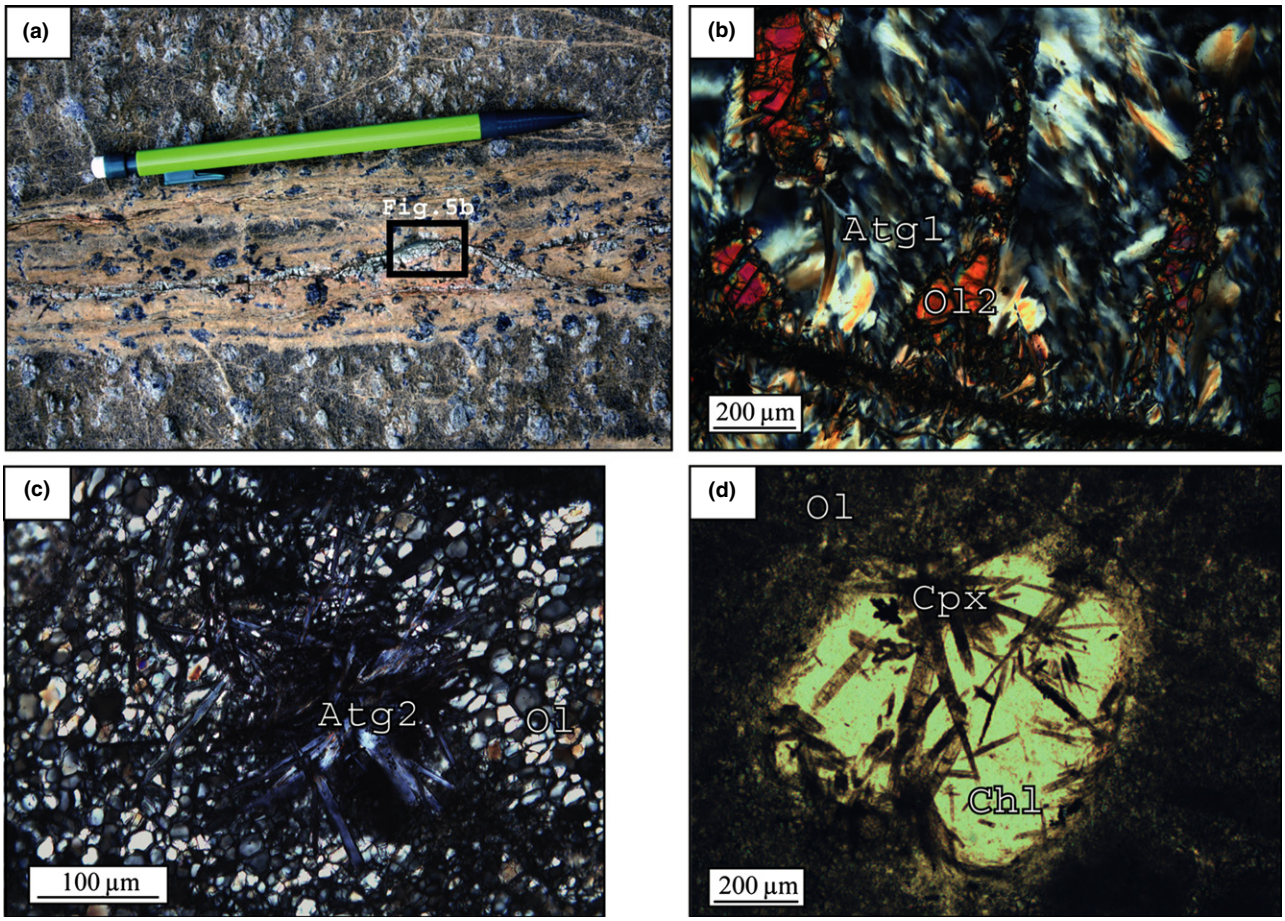

Fig. 6. (a) Network of parallel veins crossing peridotites. The vein is orange with a white centre in relief. It contains angular dark blue crystals identified in thin section as older pyroxene. (b) Microphotograph (cross polarized light) of the centre part of relief veins. Secondary olivine grows into parallel fractures cutting early antigorite. (c) Microphotograph (cross polarized light) of primary recrystallized olivine. Antigorite needles (Atg2) crystallized on that olivine. (d) Microphotograph (plane polarized light) of spinifex secondary clinopyroxene associated with chlorite. Those assemblages grow at the expense of primary recrystallized olivine.

interpret this spectrum as interstratified layers of antigorite and lizardite, suggesting that, locally, the transition lizardite to antigorite is incomplete.

In these serpentinites, the atg1 precursor is hardly preserved. Based on the Al and Cr contents, two kinds of atg1 are distinguished (Table 1): (i) high Al and Cr atg1 and (ii) low Al and Cr atg1. Assuming that the chemical composition of antigorite depends on their precursor, the group (i) corresponds to antigorite formed from pyroxene and the group (ii) corresponds to antigorite formed from olivine.

A second serpentine generation (atg2), composed of micrometric lamellae (1–10 μm), grows on atg1 (Fig. 7a). When it grows on clinopyroxene, those lamellae are oriented parallel to clinopyroxene cleavages. This suggests a late serpentinization of the clinopyroxene. The atg2 crystallization completely obliterates the previous texture. Corresponding Raman spectra are in agreement with published antigorite spectra (e.g. Auzende *et al.*, 2006).

Foliated serpentinites surrounding the massive serpentinite lens constitute the external envelope of the massif. They are composed of thin oriented lamellae of antigorite (atg2) which embed chromite within white chlorite corona, patches of chlorite, small grains of olivine and tremolite, and are associated with magnetite. The oriented lamellae of antigorite mark the foliation of the rocks.

The composition of atg2 is homogenous at the scale of the massif, except for the Cr content, which is inherited from the antigorite precursor. High Cr antigorite is formed from pyroxene and low Cr antigorite, from olivine. The Al content of atg2 is homogenous and does not depend on the antigorite precursor.

Peridotite/serpentinite contact of the Germagnano cross-section

The peridotite/serpentinite contact of the Germagnano cross-section is marked by a massive serpentinite

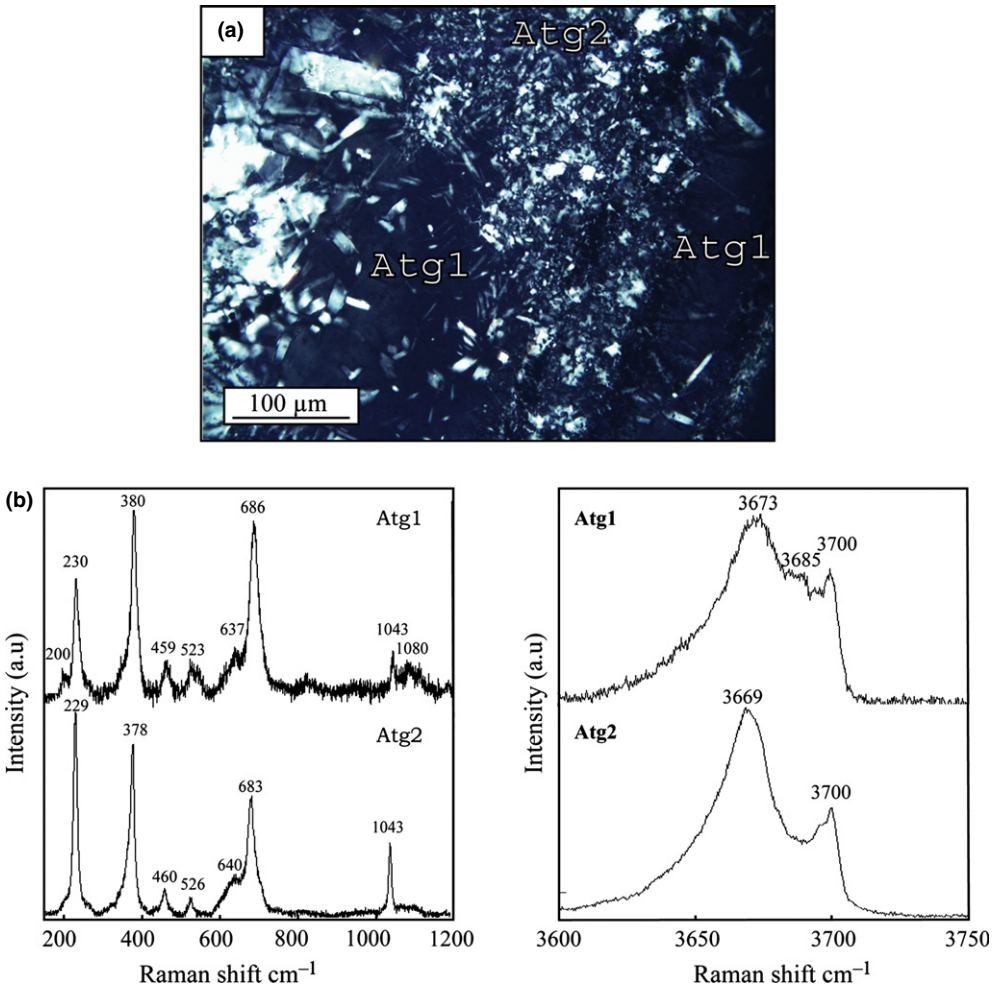

Fig. 7. (a) Microphotograph (cross polarized light) of a massive serpentinite from the Toglie cross-section. Atg2 partially replaces Atg1. (b) Raman spectrum of Atg1 and Atg2.

zone (~100 m, Fig. 2b) mostly composed of antigorite (confirmed by Raman spectroscopy; atg ~80%). Massive serpentinites contain centimetric white pseudomorphs of clinopyroxene composed of tremolite and chlorite (Fig. 8a). Clinopyroxene is rarely preserved in the centre of these aggregates. Its composition (Al_2O_3 = 4.26–5.73 wt%, Cr_2O_3 = 1.07–1.30 wt% and X_{Mg} = 0.90–0.92) is similar to primary clinopyroxene in slightly serpentinized peridotite (Fig. 4b). Metamorphic clinopyroxene crystallized as fibres intermixed with chlorite and/or tremolite (Fig. 8b) or in corona surrounding antigorite, magnetite and minute granoblastic olivine assemblages. It has lower Al_2O_3 (0.03–0.86 wt%) and Cr_2O_3 (0.02–0.40 wt%) contents than mantle clinopyroxene and a highly variable X_{Mg} (0.84–0.96, Fig. 4b). Spinel is largely recrystallized as chromite and chlorite. Orthopyroxene is no longer present in these rocks.

According to their size, two groups of olivine crystals can be identified: coarse grains of ~100 μm and minute grains of ~5 μm (Fig. 8c). Coarse olivine grains possess an irregular shape showing that they have been destabilized during serpentinization episodes. Antigorite lamellae are oriented radially around these grains. The minute olivine grains are granoblastic and surround the coarse olivine grains and the antigorite lamellae. This texture is comparable to the actual oceanic mesh texture (Fig. 8d). On Fig. 8c, the coarse olivine corresponds to the primary mantle olivine, the antigorite is formed from lizardite, and granoblastic olivine crystallized in place of antigorite and magnetite. Primary mantle olivine of massive serpentinite in the Germagnano cross-section has similar Ni contents (NiO = 0.30–0.46 wt%), higher Mn contents (MnO = 0.16–0.45 wt%) and lower X_{Mg} (X_{Mg} = 0.84–0.90) than the primitive olivine of slightly serpentinized peridotites (Fig. 4a). The composition of metamorphic olivine (NiO = 0.35–0.46 wt%, MnO = 0.26–0.40 wt% and X_{Mg} = 0.84–0.89) is similar to one of relict mantle olivine observed in the Germagnano serpentinites (Fig. 4a).

The massive serpentinites are cross cut by several veins with a width varying from several millimetres to

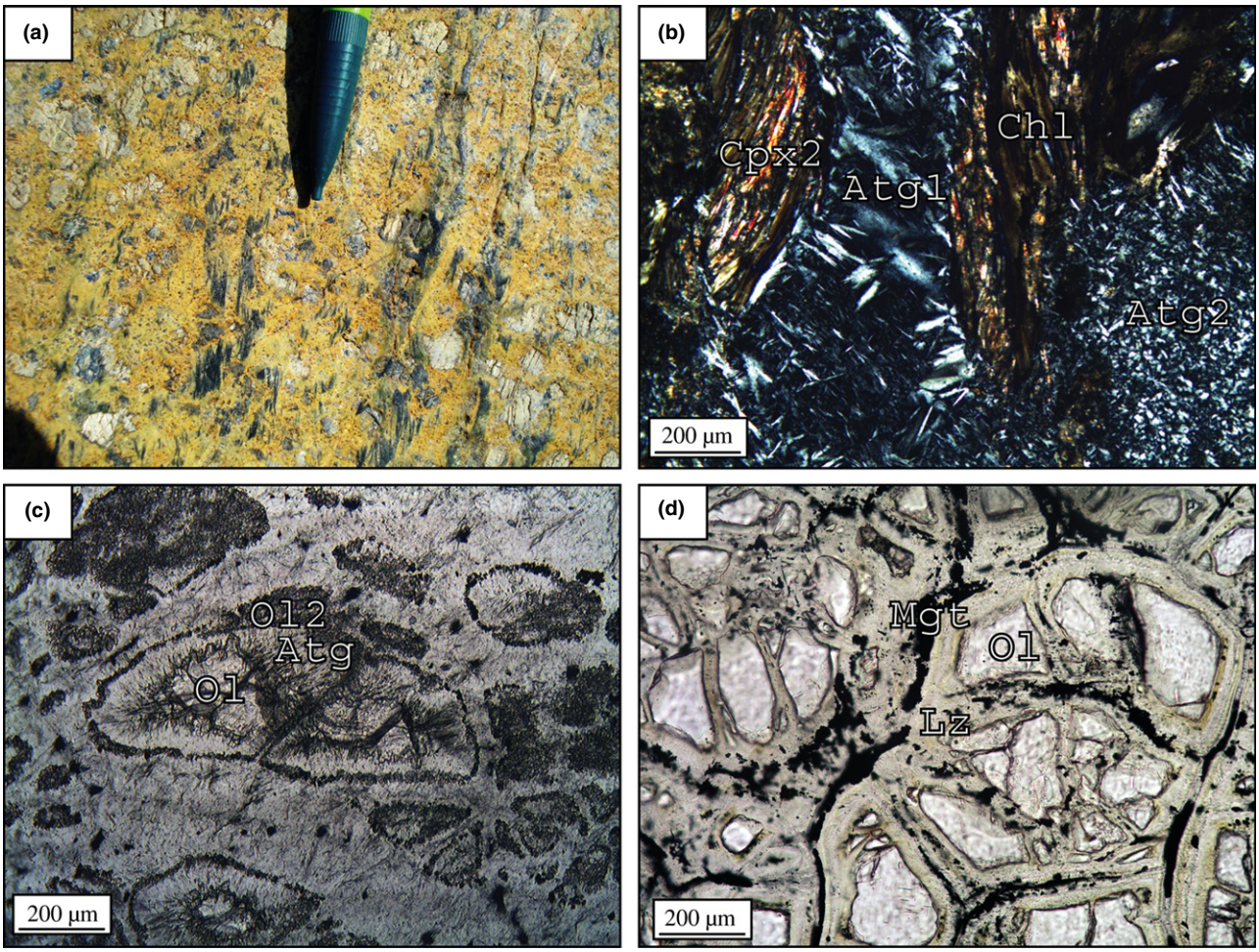

Fig. 8. (a) Massive serpentinite from the Germagnano cross-section. At the outcrop, the rock has centimetric white pseudomorphs of clinopyroxene and a network of small parallel veins. (b) Microphotograph (cross polarized light) of a small vein made of homogenous antigorite (Atg1) partially recrystallized in late antigorite lamellae (Atg2). The host rock is composed of antigorite lamellae, tremolite, chlorite and metamorphic clinopyroxene (CPx). (c) Microphotograph (plane polarized light) of an eclogitized mesh-like texture in a massive serpentinite (sample LZ27a): the centre consists of coarse olivine with an irregular shape and the rims are made of minute granoblastic olivine associated with antigorite lamellae. The two generations of olivine have the same composition. (d) Microphotograph (plane polarized light) of an oceanic serpentinite from the Mid-Atlantic ridge for comparison with (c). It shows a typical mesh as described in the literature: the mesh cells consist of a mesh rim of magnetite in string associated with lizardite and a mesh core consisting of lizardite and chrysotile with sometimes, in the centre, a primary olivine relict with straight boundaries.

centimetres (Figs 8a & 9a,b). The smaller veins (< 1 cm) are composed of homogenous areas of antigorite (Fig. 8b). The larger veins (>1 cm) are in relief and are zoned (Fig. 9b): vein centres are composed of granoblastic olivine (roughly 100 μm) associated with homogenous grey areas of antigorite (atg1) or chlorite while vein boundaries are composed of antigorite lamellae (atg2, Fig. 9c). On Fig. 9d, the homogenous grey area of antigorite is crossed by a vein of serpentine with oriented lamellae and a higher birefringence. Both textures are partially replaced by granoblastic olivine. The newly formed olivine preserves the dirty appearance of the homogenous areas, while that formed from the oriented fibres is cleaner. At the boundaries of relief veins, the antigorite lamellae grew at the expense of secondary olivine and homogenous antigorite. The following relative chronology can be established: atg1 $\Rightarrow$ secondary olivine $\Rightarrow$ atg2.

In these veins, the secondary olivine presents an unusual spectrum with additional peaks of lizardite (Fig. 9e). The NiO (0.27–0.50 wt%) and MnO (0.23–0.36 wt%) contents, and X_{Mg} (0.88–0.89) of the secondary olivine are similar to that of the host rock (Fig. 4a).

Metabasite

The slightly serpentinized peridotites of the Toglie cross-section are crossed by coarse-grained metagabbro pods and dykes, metadolerite dykes and, in a 50 m area, dykes of ultramylonitic gabbros. The metamorphic assemblages of the metabasites allows the *P–T* evolution of Lanzo massif to be constrained.

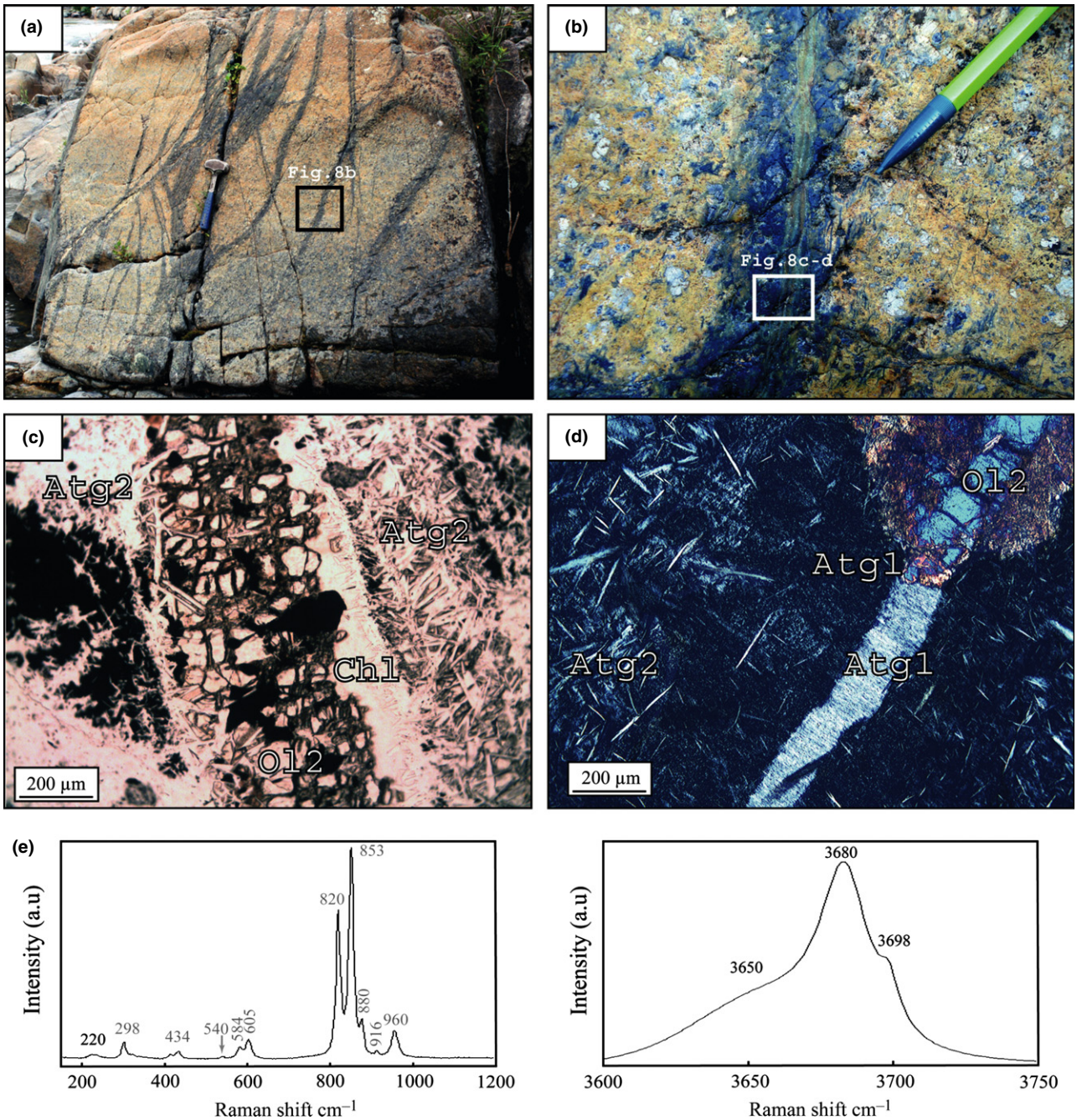

Fig. 9. Massive serpentinites from the Germagnano cross-section. (a) Massive serpentinite crossed by relief Alpine metamorphic veins. (b) Relief vein with a green and orange centre and dark blue boundaries. The contact with the host rock is diffuse. (c) Microphotograph (plane polarized light) of a relief vein crossing massive serpentinites. Vein centre is composed of granoblastic olivine and chlorite. Atg2 replaces these two minerals. (d) Microphotograph (cross polarized light) of relief veins crossing massive serpentinites. The Atg1 is crosscut by a vein of serpentine with oriented fibres and a higher birefringence. This morphological variation occurs as the vein crosses from serpentine to secondary olivine. (e) Raman spectra of secondary olivine. It possesses additional peaks (black values) that could correspond to lizardite (usual peak values of olivine are in grey).

Ultramylonitic gabbros

In a 50 m area, in the centre of the Toglie cross-section, the peridotites are crossed by a mass of ultramylonitic gabbros dykelets of several centimetres to decimetres. These dykes can isolate peridotite lenses or are emplaced in a conjugate facture system (Fig. 10a) and are connected to massive metagabbro pods.

Ultramylonitic metagabbros have a porphyroclastic texture. They consist of melanocratic bands of clinopyroxene, brown hornblende and olivine and leucocratic bands of plagioclase (Fig. 10b). Primary

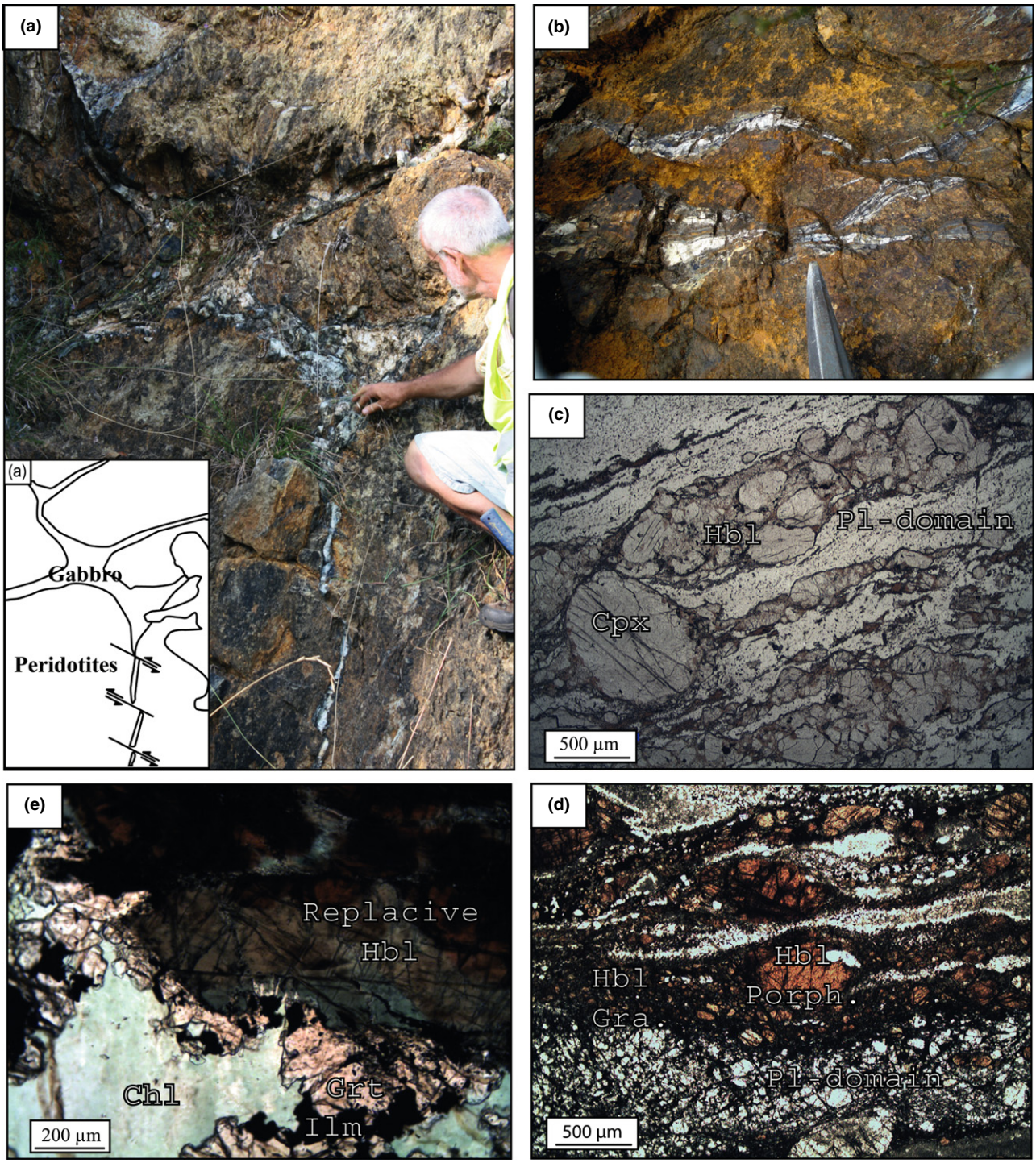

Fig. 10. (a) Ultramylonitic gabbro emplaced in a conjugate fracture system crosscutting peridotites. (b) Ultramylonitic gabbros crosscutting peridotites. They are composed of black and white bandings. (c) Microphotograph (plane polarized light) of an ultramylonitic gabbro with porphyroclasts of clinopyroxene. The layering is marked by oxide lines. Leucocrate bands are composed of fine granoblastic plagioclase. Melanocrate bands are composed of clinopyroxene porphyroclasts with pressure shadows of brown hornblende and clinopyroxene granoblasts. (d) Microphotograph (plane polarized light) of hornblende porphyroclasts (Hbl Porph.) surrounded by hornblende granoblasts (Hbl Gra.) and ilmenite (e) Microphotograph (plane polarized light) of hornblende porphyroclast zoning.

minerals are porphyroclastic and have pressure shadows composed of small grains of neoblasts of clinopyroxene and brown hornblende (Fig. 10c,d). Clinopyroxene porphyroclasts have undulatory extinction and kink bands and can contain brown hornblende blebs. The tails of clinopyroxene and

brown hornblende porphyroclasts are composed of small grains of pyroxene and/or brown hornblende and ilmenite (Fig. 10c,d). Locally, thin coronas of titanite surround the ilmenite. Olivine is totally preserved suggesting that water was absent during the later stages of metamorphic evolution. The primary plagioclase domains are recrystallized into a thin matrix of granoblastic plagioclase (< 10 μm). In the ultramylonitic gabbros, the HP metamorphism is limited to very rare coronas of garnet and chlorite surrounding hornblende porphyroclasts or fine-grained aggregates of jadeite, quartz and needles of zoisite in the plagioclase domain.

The main mineralogical assemblages of ultramylonitic gabbros correspond to a low-pressure (LP) assemblage acquired during the cooling of magma. The temperature of these LP parageneses can be calculated using the amphibole thermobarometer of Ernst & Liu (1998), based on Ti content of the M2 site that increases with increasing temperature. The use of Ti thermometer requires an excess of Ti in the system. We assume that this condition is realized when Ti is present as an oxide (ilmenite, rutile) or in titanite. The accuracy of this thermometer has been estimated at the Institut für Mineralogie (Hannover, Germany) using published and unpublished experimental data, and temperature estimates are accurate to $\pm 40°$ (J. Koepke, pers. comm.). However, Ti content is always higher when amphibole is in contact with ilmenite; thus, these values were not used for calculations.

Hornblende is divided into four types. (i) Hornblende blebs consist of minute grains of 10 μm enclosed within igneous clinopyroxene and are generally elongated parallel to pyroxene cleavages. Its composition is highly titaniferous (TiO_2 = 4.40–4.79 wt%, Table 2, Fig. 11) and corresponds to temperatures ranging from 1020 to 1030 °C. (ii) Porphyroclastic brown hornblende is centimetric and has an irregular zoning from dark to light brown depending on its TiO_2 content (4.15–5.25 wt%, Fig. 11). The estimated formation temperature varies from 1010 to 1030 °C. (iii) Locally, the porphyroclastic brown hornblende rims can be zoned from brown to green over 500 μm (Fig. 10e). The TiO_2 contents of replacive amphibole vary from 3.61 wt% for the light brown hornblende to 0.32 wt% for green hornblende (Table 2 & Fig. 11). Those temperatures of formation correspond to cooling from 990 to 560 °C. The porphyroclastic and replacive hornblendes are crossed by HP veins of chlorite and clinopyroxene ~20 μm long needles suggesting that their formation is oceanic. (iv) The tails of porphyroclastic hornblende and clinopyroxene are composed of fine aggregates of granoblastic brown hornblende, clinopyroxene and ilmenite. The TiO_2 contents of hornblende granoblasts vary from 3.67 to 4.38 wt% (Fig. 11), which correspond to a formation temperature from 990 to 1020 °C (Table 2).

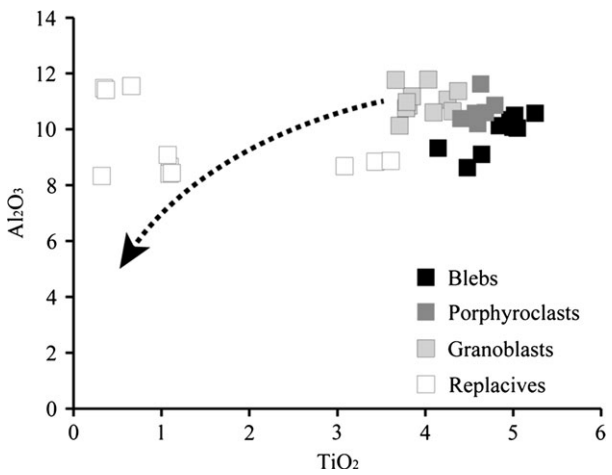

Fig. 11. TiO_2 (wt%) *v.* Al_2O_3 (wt%) contents of hornblende from mylonitic gabbros. The black dotted arrow shows the theoretical evolution of TiO_2 and Al_2O_3 contents of hornblende predicted by Ernst & Liu (1998) model during the isobaric cooling of the oceanic lithosphere.

In the thermobarometer of Ernst & Liu (1998), pressure is obtained by combining the Al_2O_3 content with the TiO_2 content of amphibole. In the ultramylonitic metagabbros of Lanzo massif, the Al_2O_3 content is constant in the different hornblende types (Fig. 11, $Al_2O_{3(blebs)}$ = 10.19–11.62 wt%, $Al_2O_{3(porphyroclasts)}$ = 8.62–10.57 wt%, $Al_2O_{3(granoblasts)}$ = 9.35–11.77 wt%, $Al_2O_{3(replacives)}$ = 8.32–11.47 wt%), while the TiO_2 is variable. The high-Ti hornblende records pressures ranging from negative pressure to 0.4 GPa. Those estimates are poor, but coherent with the emplacement of the gabbros at LP in the oceanic lithosphere. However, the pressure estimates for replacive hornblende range from 0.3 to 1.7 GPa. The model of Ernst & Liu (1998) predicts a diminution of Al_2O_3 content with TiO_2 content during the isobaric cooling of the oceanic crust (Fig. 11). Ernst & Liu (1998) suggest that, during oceanic cooling, the replacive hornblende exsolves TiO_2 as ilmenite (Fig. 10e), while the Al_2O_3 is not redistributed explaining those overly HPs.

Metagabbros and dolerites

Two kinds of metagabbro pods along the Toglie cross-section were observed, foliated and massive metagabbros. Foliated metagabbros are composed of green millimetric to centimetric jadeitic clinopyroxene and white areas corresponding to the plagioclase domain (Fig. 12a). They have a foliation varying from N030 to N050 with a dip of E70. Meta-doleritic dykes with planar structure, parallel to the selvages and interpreted as magmatic fluidity, crosscut the foliation of metagabbro pods (Fig. 12b). This demonstrates that the deformation of these metagabbros, along with ultramylonitic gabbros, is oceanic.

Massive metagabbros record a HP metamorphism that induced a partial or total recrystallization of

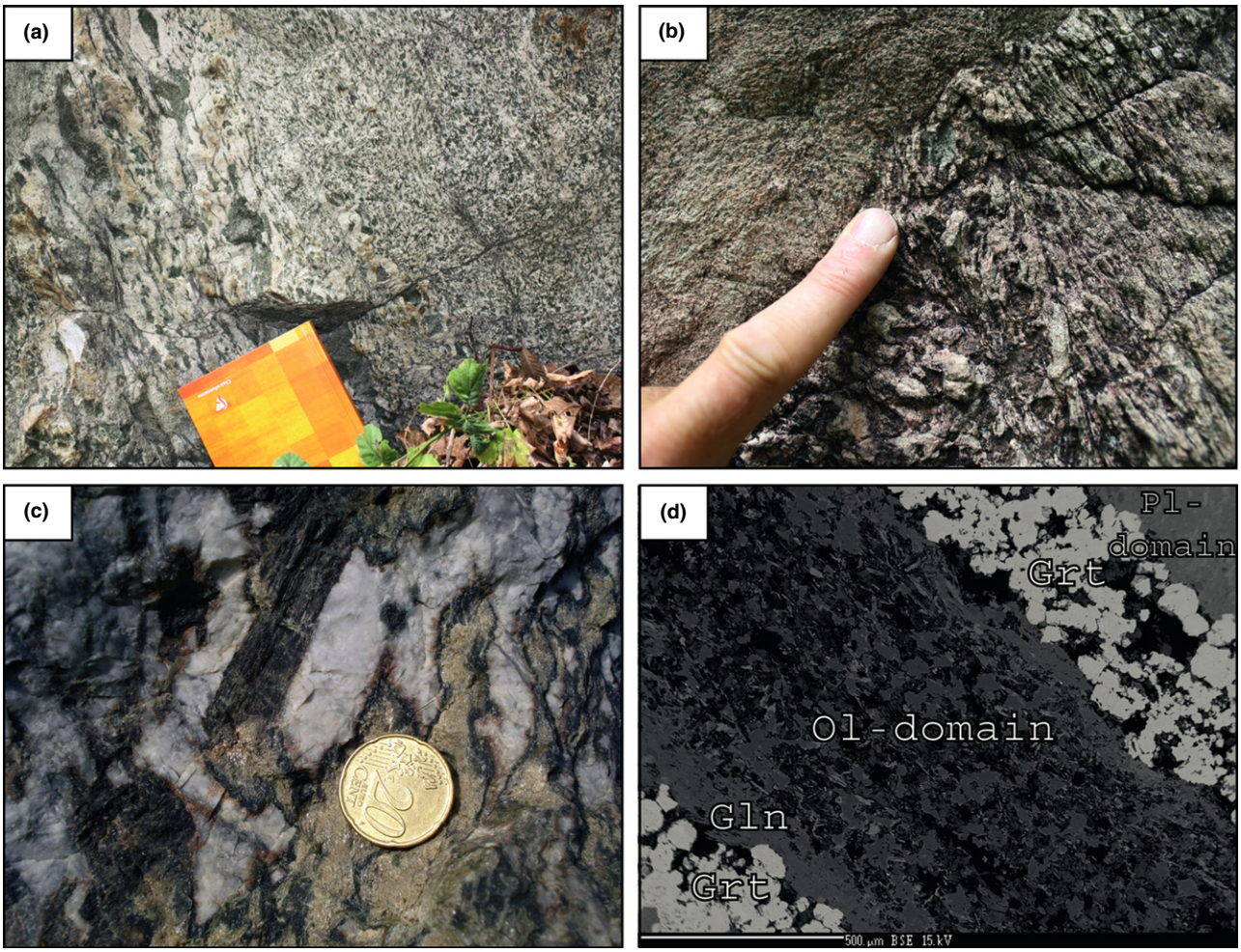

Fig. 12. (a) Foliated metagabbros made of green jadeitic crystals and a white matrix. The crystal size varies rapidly from the millimetre to the centimetre. (b) A dyke of metadolerite with a flow structure crosscutting foliated metagabbro pod. (c) Coarse grain metagabbro. Olivine domains are brown/yellow. In contact with the plagioclase domain, they show a black corona of glaucophane and a red corona of garnet. Black prisms of magmatic pyroxene are preserved. (d) Backscattered electron image of a coarse grain metagabbro. The olivine domain (Ol-domain) is separated from plagioclase domain by a double corona of glaucophane and garnet.

magmatic domains. The plagioclase domain is highly recrystallized into HP microcrystalline assemblages mostly composed of epidote needles of 20–50 μm, jadeite/omphacite, quartz and kyanite grains of 20 μm. Occasionally, in the centre of the microcrystalline aggregate, the jadeite/omphacite and quartz are partially destabilized into fine crystallized areas of oligoclase. Primary magmatic augite (Table 3) can be preserved as black centimetric prisms (Fig. 12c). Mostly, it is replaced by actinolite crystals of ~50 μm diameter surrounded by a glaucophane corona of ~10 μm width. The actinolite crystals are oriented in the clinopyroxene domain suggesting an epitaxial crystallization of the amphibole from the clinopyroxene. Olivine domains are composed of microcrystalline aggregates of tremolite, chlorite, omphacite, glaucophane, talc and quartz of ~50 μm in diameter. The olivine and plagioclase domains are separated by a double corona composed of black micrometric glaucophane crystals towards olivine and of rounded red garnet crystals of ~200 μm in diameter towards plagioclase (Fig. 12d).

The primitive domains of the metagabbros have been replaced by micrometric assemblages containing garnet and omphacite. To constrain the equilibration temperature of the metagabbros, the thermometers of Ellis & Green (1979) and Powell (1985), based on Mg/Fe exchange between omphacite and garnet were used. The garnet displays a slight chemical zoning from core to rim (Table 3) and the composition of omphacite microcrystals is homogenous at millimetric scale (Table 3) suggesting that those minerals are in equilibrium at this scale. The garnet/omphacite couples were selected in a 100 μm^2 area. Ryburn *et al.* (1975) have shown that a significant amount of Fe^{3+} in clinopyroxene composition can cause a large error in temperature calculation. The Fe^{3+} content of omphacite was estimated by stoichiometry to determinate

Table 3. Microprobe analysis of metagabbros minerals separated by crystallographic domains. Cations are normalized to four oxygen for olivine, six oxygen for clinopyroxene and 28 oxygen for chlorite.

	Ol-domain								Cpx domain Act			Pl-domain				
	Grt core	Grt rim	Gln	Tlc	Act	Chl	Cpx	Cpx	Cpx	Act	Gln	Pg	Gln	Ep	Cpx	Ky
SiO_2	38.74	38.95	60.02	62.02	56.02	29.86	55.18	56.54	54.81	57.67	58.35	47.76	58.32	40.24	59.56	37.54
TiO_2	0.09	0.01	0.00	0.03	0.07	0.00	1.57	0.11	0.05	0.00	0.05	0.06	0.07	0.07	0.00	0.01
Al_2O_3	21.94	22.07	12.36	0.74	1.69	20.20	8.10	9.94	0.32	1.00	10.44	40.71	11.59	32.90	24.26	62.94
FeO	27.42	27.45	4.44	5.01	7.36	13.47	3.76	3.34	5.34	5.84	6.69	0.22	7.06	0.88	0.72	0.12
MnO	0.89	0.65	0.05	0.02	0.07	0.13	0.10	0.00	0.17	0.08	0.06	0.00	0.04	0.00	0.02	0.03
MgO	4.59	4.75	13.12	27.59	18.51	25.11	10.56	10.12	15.46	20.05	13.13	0.30	12.44	0.01	0.96	0.01
CaO	7.38	7.86	0.75	0.05	11.92	0.01	16.10	14.52	24.40	12.52	2.93	0.12	2.11	24.62	1.88	0.06
Na_2O	0.00	0.01	7.01	0.15	0.75	0.00	5.09	6.00	0.15	0.56	5.85	7.35	6.31	0.09	13.32	0.00
K_2O	0.02	0.00	0.00	0.11	0.03	0.06	0.01	0.02	0.00	0.00	0.01	0.40	0.01	0.00	0.03	0.00
Cr_2O_3	0.00	0.00	0.07	0.00	0.00	0.04	0.00	0.02	0.03	0.03	0.11	0.00	0.00	0.02	0.06	0.00
Total	101.07	101.75	97.83	95.80	96.46	88.93	100.49	100.64	100.72	97.75	97.66	96.92	97.95	98.83	100.82	100.70
Si	6.00	5.99	7.98	7.98	7.93	5.79	1.97	1.99	2.00	7.99	7.92	5.98	7.89	3.03	2.00	4.03
Ti	0.01	0.00	1.94	0.11	0.28	4.62	0.34	0.41	0.01	0.16	1.67	6.01	1.85	2.92	0.96	0.00
Al	4.01	4.00	0.00	0.00	0.01	0.00	0.04	0.00	0.00	0.00	0.00	0.01	0.01	0.00	0.00	7.95
Fe^{2+}	3.55	3.53	0.49	0.54	0.87	2.18	0.11	0.10	0.16	0.68	0.76	0.02	0.80	0.00	0.02	0.01
Fe^{3+} [a]	< 0.01	0.01					< 0.01	< 0.01	< 0.01						< 0.01	
Mn	0.12	0.08	0.01	0.00	0.01	0.02	0.00	0.00	0.01	0.01	0.01	0.00	0.00	0.00	0.00	0.00
Mg	1.06	1.09	2.60	5.29	3.91	7.26	0.56	0.53	0.84	4.14	2.66	0.06	2.51	0.00	0.00	0.00
Ca	1.23	1.30	0.11	0.01	1.81	0.00	0.62	0.55	0.95	1.86	0.43	0.02	0.31	0.00	0.00	0.01
Na	0.00	0.00	1.81	0.04	0.20	0.00	0.35	0.41	0.01	0.15	1.54	1.78	1.65	0.00	0.05	0.00
K	0.00	0.00	0.00	0.02	0.01	0.02	0.00	0.00	0.00	0.00	0.00	0.06	0.00	0.00	0.87	0.00
Cr	0.00	0.00	0.01	0.00	0.00	16.00			0.00	0.00	0.01	0.00	0.00	0.00	0.07	
OH			2.00	4.00	2.00	0.01	0.00	0.00		2.00	2.00	4.00	2.00	1.00	0.00	
Total	15.98	16.01	16.95	17.98	17.02	35.90	4.00	4.00	3.99	17.00	17.00	17.94	17.01	7.01	3.96	12.00

[a]Estimated by stoichiometry.

the distribution coefficient between clinopyroxene and garnet.

Temperatures obtained are between 540 (at 0.5 GPa) and 590 °C (at 2.5 GPa) for the Ellis & Green (1979) thermometer and between 520 (at 0.5 GPa) and 560 °C (at 2.5 GPa) for the Powell (1985) thermometer. From these values, the barometer of Holland (1983), based on jadeite content of omphacite, was used. This barometer depends on albite ⇒ jadeite + quartz reaction. However, albite is no longer present in the samples, and so the 1.36–1.78 GPa range given by the Holland (1983) barometer is a minimum estimate. Pelletier & Müntener (2006) indicated a peak of metamorphism at 550–620 °C and 2.0–2.5 GPa for the Lanzo massif. These values were obtained for kyanite + talc + chloritoid and talc + chloritoid + garnet domains in metagabbro dykes by thermodynamic calculation (see Pelletier & Müntener, 2006 for further details). Although our temperature and minimum pressure estimates are in agreement with those of Pelletier & Müntener (2006), their more precisely constrained values will be used as the reference values for the metamorphic peak.

DISCUSSION

The magmatic and metamorphic evolution of the metagabbros

The succession of different serpentine generations permits the reconstruction of a qualitative *P–T* path of oceanic cooling, subduction and then exhumation. The early emplacement of gabbros and dolerites in the peridotites means that they have recorded the same metamorphic evolution as ultramafic rocks and allows the *P–T* path of the massif to be quantified. Two contrasting parageneses have been found in these magmatic rocks. Dykes of mylonitic gabbros are composed of clinopyroxene, olivine, plagioclase, hornblende, ilmenite and titanite. This corresponds to a LP and high-temperature (HT) paragenesis; the high-pressure–low-temperature (HP–LT) metamorphic overprint is very limited in these rocks. On the other hand, the paragenesis of metagabbro pods is mainly eclogitic with a few LP mineral assemblages consisting of actinolite, chlorite, albite and epidote and a few relicts of magmatic augite.

Lanzo (meta)gabbros have MORB compositions (Bodinier, 1988) demonstrating their oceanic origin. In the mylonitic gabbros, the porphyroclastic brown hornblende displays high TiO_2 contents (4.15–5.25 wt%) showing that they are magmatic. The formation of hornblende blebs enclosed into magmatic porphyroclasts of clinopyroxene suggests that they formed by silicate melt trapped during magmatic crystallization (Coogan *et al.*, 2001). This is consistent with their TiO_2 contents (4.40–4.79 wt%) that correspond to suprasolidus formation temperature (1020–1030 °C).

The TiO_2 content of hornblende granoblasts (3.67–4.38 wt%) is lower than that of magmatic porphyroclasts and blebs (Fig. 11). Corresponding temperature estimates are between 990 and 1020 °C. Thus, the dynamic recrystallization, which leads to the formation of the hornblende granoblasts, occurs at HT just after the crystallization of the magma. It suggests that the

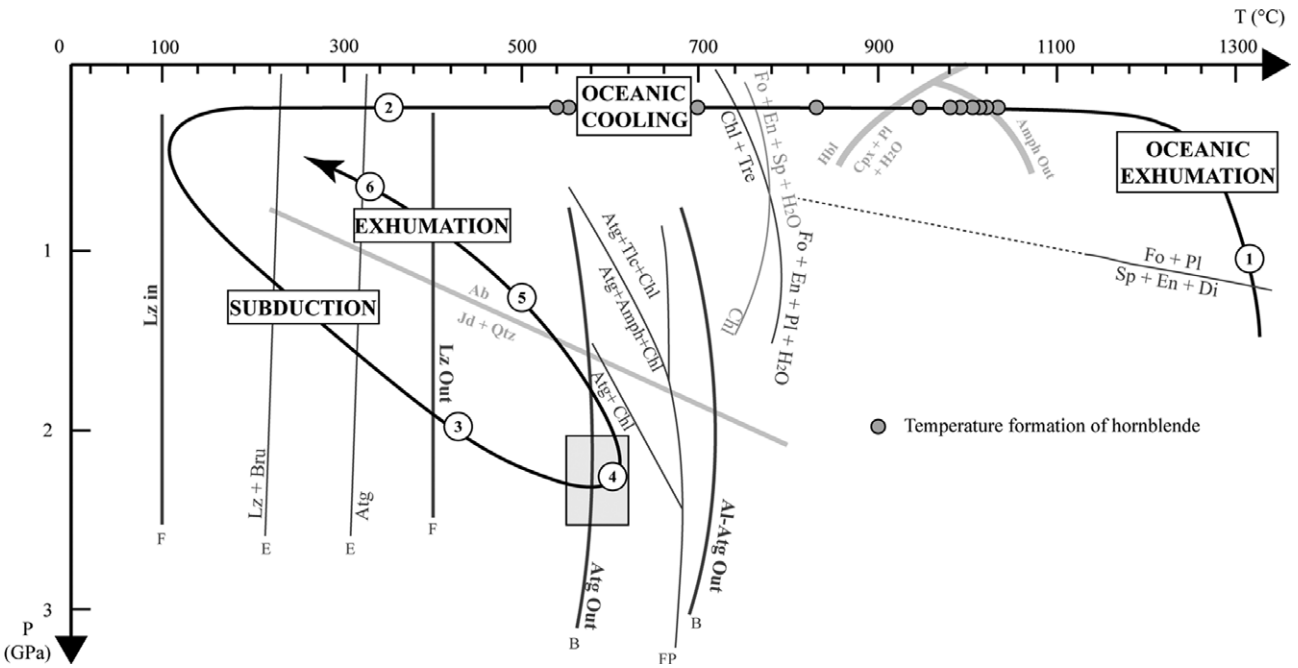

Fig. 13. *P–T* path of mafic and ultramafic rocks of the Lanzo massif. During oceanic exhumation in an OCT context, the mantle passes the transition from spinel lherzolite to plagioclase lherzolite (1). Then, during LP cooling (2), the peridotites and the metagabbros cross, in the presence of H_2O, successive reactions leading to the disappearance of primary phases (olivine, pyroxene and plagioclase). At high temperature (HT), the mylonitic gabbros record the beginning of the cooling of the oceanic lithosphere: grey bold dots correspond to hornblende temperature estimates (Table 2). At lower temperature, plagioclase and spinel react with pyroxene and olivine to form chlorite and chlorite/tremolite assemblages. From 400 °C, peridotites are partially to fully serpentinized to lizardite (2) at the expense of olivine and orthopyroxene (F: Martin & Fyfe, 1970). During alpine subduction (3), the lizardite breaks down to antigorite (E: Evans, 2004). In the metagabbros, the prograde metamorphism is marked by the destabilization of igneous and LP/low-temperature (LT) metamorphic phases to high-pressure/HT phases of eclogite facies. At *P–T* metamorphic peak (4), Al-poor serpentine is replaced by secondary olivine (B: Bromiley & Pawley, 2003) and the paragenesis Cpx + Chl +/− Amph is stable in ultramafic rocks (FP: Fumagalli & Poli, 2005). During the retrograde path, a new antigorite generation is formed at the expense of other phases (5) while in metagabbros quartz and jadeite are transformed into albite. A later serpentinization step could correspond to the crystallization of antigorite and lizardite micro-phases (6) on secondary olivine at LP/LT.

magma has been emplaced in fractures of the lithosphere during tectonic activity.

The rare zoning of hornblende porphyroclasts from light brown to green with low TiO_2 content (0.32–3.61 wt%) indicates that water circulation was limited after the HT stage and the mylonitic gabbros record little evidence of the cooling of the lithosphere.

In the metagabbro pods, the crystallization of LP (actinolite and chlorite) and then HP assemblages (omphacite, garnet, kyanite, talc, glaucophane, zoisite and quartz) at the expense of igneous or previous LP phases reveals an evolution from greenschist facies conditions to eclogite facies conditions. Phase relationships of these different facies allow us to propose the following geodynamic evolution (Fig. 13): (i) actinolite, hornblende, tremolite and chlorite crystallization at the expense of igneous phases are attributed to LP oceanic metamorphism during oceanic exhumation. As is classically described (e.g. Messiga & Tribuzio, 1991), olivine, reacting with plagioclase, is replaced by chlorite/tremolite aggregates, whereas augite is replaced by actinolite and/or green hornblende during oceanic lithosphere cooling. (ii) During subduction, the crystallization of HP assemblages (omphacite, garnet, kyanite, talc, glaucophane, zoisite, quartz) at the expense of igneous and LP metamorphic phases is attributed to the burial of the massif to eclogite facies conditions. (iii) Retrograde evolution during massif exhumation, from subduction to a collision context, is limited to a discrete omphacite destabilization into albite and epidote.

The HP–LT metamorphism of the gabbros is controlled by the presence of hydrous oceanic phases. Ultramylonitic metagabbros do not record the alpine metamorphism because the water circulation might have been limited in these rocks during oceanic spreading. On the other hand, the metagabbro pods largely record the Alpine metamorphism, with the crystallization of HP hydrous phases (glaucophane, talc). This suggests that metagabbro pods were hydrated and largely metamorphosed during oceanic step.

Three steps of serpentinization in ultramafic rocks

According to field work observations and the *P–T* path obtained from the associated metagabbros, the ultramafic rocks of Lanzo massif have recorded four geodynamic steps (Fig. 13): (i) oceanic exhumation of the

peridotite in OCT context; (ii) ocean floor cooling and partial hydration; (iii) subduction; and (iv) exhumation during subduction or continent collision. The different geodynamic steps produced three serpentine generations in the ultramafic rocks.

Plagioclase dykelets and coronas surrounding spinel show that spinel peridotites of Lanzo massif are partially equilibrated in the plagioclase lherzolite domain and intruded by basic magmas during massif oceanic exhumation in an OCT context (Bodinier, 1988; Muntener *et al.*, 2004; Piccardo *et al.*, 2007). This event is rarely preserved because plagioclase is destabilized during oceanic expansion or subduction: in most rocks, it is recrystallized into chlorite and actinolite and/or into garnet, zoisite and omphacite assemblages.

Serpentinite resulted from hydrothermal alteration of ultramafic rocks at 100 °C < T < 700 °C (Bromiley & Pawley, 2003; Andreani *et al.*, 2007). During oceanic expansion, peridotites, in contact with oceanic water, at temperatures below 400 °C (Agrinier & Cannat, 1997; Bach *et al.*, 2004), were largely hydrated and transformed into serpentinite mostly composed of lizardite (Mével, 2003; Evans, 2004; Andreani *et al.*, 2007). This step is largely preserved in slightly serpentinized peridotites where lizardite crystallizes in veins crossing the olivine and orthopyroxene and locally, when the hydration is more important, into mesh and bastite texture (Viti & Mellini, 1998). Slightly serpentinized peridotites also contain antigorite veins growing across lizardite veins and primary minerals. Even if lizardite/antigorite transition does not depend much on pressure, it is admitted that antigorite is the higher pressure form of the serpentine (Scambelluri *et al.*, 1995; Ulmer & Trommsdorff, 1995; Wunder & Schreyer, 1997; Auzende *et al.*, 2006; Groppo & Compagnoni, 2007). Thus, this structural relationship suggests that lizardite recrystallization into antigorite occurs during the alpine subduction.

In ultramafic rocks, the two antigorite generations (atg1 and atg2) are separated by the crystallization of secondary olivine.

(1) The first generation of antigorite (atg1) crystallized from all previous minerals. In massive serpentinites, it is sometimes represented as an intermediate Raman spectrum between lizardite and antigorite. This suggests that, in serpentinites, the alpine serpentinization (antigorite) overprints the oceanic serpentinization (lizardite, Fig. 13).
(2) The secondary olivine grew from the early antigorite in the slightly serpentinized peridotites and in massive serpentinites. This antigorite breakdown into olivine has already been observed in previous works (Scambelluri *et al.*, 1995; Trommsdorff *et al.*, 1998; Hermann *et al.*, 2000; Nozaka, 2003; Padron-Navarta *et al.*, 2008), where it was interpreted as antigorite dehydration during prograde metamorphism (Fig. 11). The crystallization of secondary olivine is associated with chlorite, but never with orthopyroxene. This suggests that the classical reaction Atg = Ol + Opx + H_2O (e.g. Garrido *et al.*, 2006) is incomplete in the Lanzo massif.
(3) A late antigorite (atg2) crystallized from previous minerals (primary minerals, early antigorite and secondary olivine) in the massive and foliated serpentinites. Its crystallization could correspond to a retrograde serpentinization episode during massif exhumation (Fig. 13). This serpentinization step is accompanied by a strong deformation obliterating previous structures at outcrop and thin-section scale.

The HP stability of antigorite relative to secondary olivine is controlled by its composition. According to Bromiley & Pawley (2003), a few wt% of Al_2O_3 in antigorite is enough to stabilize its structure at higher temperatures and pressures: low Al antigorite is stable until 550 °C while high Al antigorite break down is completed at higher temperature (700 °C). In the ultramafic rocks of the Lanzo massif, the *P–T* conditions of peak metamorphism (2.0–2.5 GPa and 550–620 °C) is in the divariant field over which antigorite breaks down into enstatite + olivine + chlorite + H_2O (Fig. 13). The absence of orthopyroxene suggest that this dehydration reaction may be stopped after an intermediate step.

Microprobe analysis of mantle and secondary olivine in ultramafic rocks shows significant variation in MnO content and X_{Mg} as a function of rock lithology (peridotite or serpentinite). These compositional variations are summarized in Fig. 4a. The MnO content of olivine increases progressively from peridotite to serpentinite while the X_{Mg} decreases. This suggests that its composition was modified by external fluid during oceanization. However, in each rock type, it is impossible to distinguish the two olivine groups: there is an overlapping range of composition between primary and metamorphic olivine. The similar composition of mantle and secondary olivine in the serpentinites or peridotites suggests that the serpentinization and deserpentinization processes during subduction evolved in a closed system. As suggested in Fig. 8c, the formation of metamorphic olivine requires the involvement of Fe-oxide (magnetite) during antigorite breakdown. In that case, the metamorphic olivine composition can be explained by the reaction: magnetite + antigorite ⇒ olivine2 + H_2O.

In the same way, other secondary minerals can be associated with this dehydration step. Metamorphic clinopyroxene crystallization was observed coexisting with tremolite and/or chlorite. Fumagalli & Poli (2005) observed experimentally this three-phase assemblage at similar *P–T* conditions (2.2 GPa and 700 °C) in olivine-poor lherzolite.

The retrograde evolution is essentially marked by the crystallization of a late antigorite in the massive

and foliated serpentinites composing the envelope of the massif. The Raman spectra of secondary olivine are associated with a serpentine structure (lizardite or antigorite). The origin of this serpentine micro-phase remains unclear. It could represent relicts of the prograde serpentine that is destabilized into secondary olivine at the metamorphic peak. On the other hand, it could be interpreted as retrograde serpentine crystallization on secondary olivine, during massif exhumation, reacting with just the water contained in this olivine. Indeed, it has been shown, in mantle peridotite xenoliths (Matsyuk & Langer, 2004) and in experimental studies (e.g. Keppler & Bolfan-Casanova, 2006), that a 'large' amount of water can be dissolved in olivine. Solubility of water in olivine is function of temperature, pressure and olivine composition (Zhao *et al*., 2004; Keppler & Bolfan-Casanova, 2006). At *P–T* conditions similar to the peak of Lanzo metamorphism, Mosenfelder *et al*. (2005) showed that olivine can contain up to 375 ppm of water. Thus, the late crystallization of serpentine on secondary olivine could be the result of olivine re-equilibration to lower *P–T* during massif exhumation.

The prograde evolution is well preserved in massive ultramafic rocks that provide a good reconstitution of the different serpentinization steps. On the other hand, the formation of the retrograde antigorite is abundant in the foliated serpentinite of the envelope. In this zone, the deformation increases the reaction kinetics and leads to the obliteration of all previous textures and the prograde history.

The serpentinization front of the Lanzo massif: a preserved palaeo-Moho of slow spreading ridge

The Lanzo massif preserved its oceanic sedimentary cover and ophicarbonate during subduction (Lagabrielle *et al*., 1989; Pelletier & Müntener, 2006) attesting that it constituted the oceanic floor of the Palaeo-Tethys and that the serpentinization started during an oceanic step. This is confirmed by the presence of early lizardite in the slightly serpentinized peridotite (Fig. 3b). Furthermore, the petrological study shows that the massive serpentinites, defining the front of serpentinization, preserved eclogitized characteristic textures of the oceanic alteration (Fig. 8c) and traces of lizardite within prograde antigorite structure (Fig. 7b). This testifies that the eclogitized serpentinization front of the Lanzo massif is inherited from the oceanic alteration and constitutes a palaeo-Moho. This is in good agreement with the thickness of the external envelope of serpentinite of 3–5 km that is similar to the thickness of a serpentinized oceanic lithosphere (3–6 km). However, the seismic profiles carried out in intra-oceanic context show a progressive increase of the seismic speed with depth which is interpreted as a progressive increase of mantle serpentinization, from the mantle peridotites to the ocean floor (Fig. 14). In the Lanzo massif, the peridotite/serpentinite limit is sharp: the peridotites are completely serpentinized from the supposed paleo-oceanic floor, marked by the presence of ophicalcites, to the slightly serpentinized peridotites at the serpentinization front.

The rheological behaviour of a serpentinized peridotite depends on its serpentinization degree. The presence of 15% serpentine reduces the strength of an altered peridotite to that of a pure serpentine (Escartin *et al*., 2001). Thus, the 15% serpentinization horizon located at a depth of ~3 km in the oceanic lithosphere (Fig. 14; Canales *et al*., 2000) constitutes a mechanical decoupling layer. This layer can correspond to the serpentinite/peridotite limit in the Lanzo massif, beneath which the slightly serpentinized peridotites (< 20%) have been preserved from deformation, thus preserving oceanic textures. Above this layer, the serpentinized peridotites (serpentinization > 20%) of the oceanic lithosphere constitutes a less competent level with a rheological behaviour similar to that of pure serpentine that should preferentially accommodate the deformation from oceanic (Escartin *et al*., 2001) to subduction context (Chernak & Hirth, 2010). During subduction and then exhumation, this deformation zone also favours water circulation and the completion of the serpentinization reactions; the new serpentinization stage of the peridotite minerals obliterating the oceanic serpentinization gradient (Fig. 14). As suggested by the similar composition of primary and metamorphic olivine (Fig. 4a), the massif could have evolved in a relatively closed system during subduction. Indeed, the lizardite to antigorite transition is a dehydration reaction, which released new fluid, permitting the following serpentinization process without any new external provision of fluid.

As suggested by this study, the subduction and the exhumation of the oceanic lithosphere are influenced by its initial structure. Most of the alpine ophiolites came from the Tethyan Ocean, which is an analogue to the modern central Atlantic Ocean (Lagabrielle & Cannat, 1990; Cannat *et al*., 1995). Indeed, remnants of oceanic lithosphere are sometimes rich in magmatic rocks (e.g. MonViso) and sometimes made of serpentinized mantle peridotites, almost exclusively (e.g. Monte Maggiore, Corsica or Lanzo). During subduction, the oceanic structure influences the location of rheological threshold and corresponding decollement permitting the exhumation of the ophiolite. For the magmatic unit, the decollement occurs at the base of gabbroic crust (e.g. MonViso, Angiboust *et al*., 2011). For a partially serpentinized peridotite unit, the decollement should occur close to the serpentinization front. This explains why serpentinites are rarely associated with peridotites in the Alps. The Lanzo massif is thus an exceptional case where the serpentinization front and the oceanic structure of the OCT are preserved during the subduction.

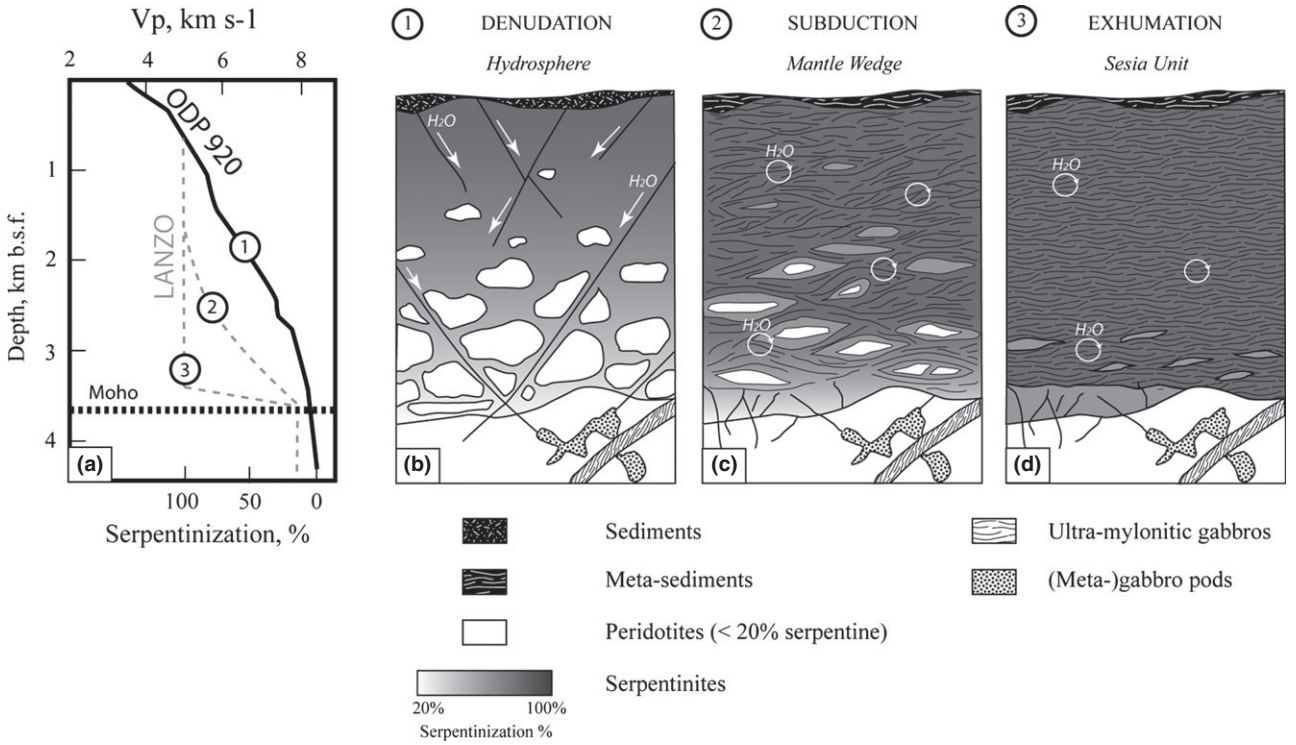

Fig. 14. Conceptual model for the evolution of the oceanic serpentinization front of the ultramafic Lanzo massif during alpine subduction and exhumation. (a) Seismic velocity profile observed across the Mid-Atlantic Ridge at the 920 ODP site (black line, modified after Andreani *et al.*, 2007) compared to the hypothetic evolution of seismic velocity profile of Lanzo massif (dotted grey line). The Moho (dotted black line) is defined by a velocity of 8 km s^{-1}. The progressive increase of P wave velocity with depth, in an oceanic context, is interpreted as a gradient of serpentinization affecting the mantle. (b) Interpretative schema produced from velocity seismic profiles across the Mid-Atlantic Ridge at 920 ODP site. (c) During subduction, the deformation principally affects the serpentinization zone where more competent levels form lenses. In this zone, the deformation would make the transformation from lizardite to antigorite and fluid circulation easier. That would permit a more pervasive serpentinization of the slightly serpentinized zone. (d) During retrograde exhumation, intense deformation and dehydration continue. The more competent zone (peridotite) will be totally transformed in retrograde antigorite forming lenses of massive serpentinites surrounded by foliated serpentinites. The front of serpentinization is not significantly displaced during prograde and retrograde serpentinization.

CONCLUSIONS

According to the metamorphic history of the Lanzo massif, three serpentine generations have been identified in ultramafic rocks. The first one is characterized by the crystallization of the low *P–T* serpentine species (lizardite) with other accessory phases (magnetite), formed in oceanic context, and preserved in slightly serpentinized peridotites. This serpentinization episode is the most extensive. The serpentinization front dates from this event. During subduction, a prograde antigorite replaced the lizardite and to lesser extent primary minerals of peridotites: this episode affected preferentially the serpentinites. The final stage of this step is marked by the incipient deserpentinization of antigorite to secondary olivine (and clinopyroxene, chlorite and tremolite) at the peak *P–T* conditions. During exhumation of the massif, the pervasive deformation completely obliterated the previous textures of minerals which are reoriented according to the strong foliation formed by the crystallization of retrograde antigorite in massive and foliated serpentinites.

On the basis of petrological and field work observations, we propose that the serpentinite to peridotite transition corresponds to a palaeo-Moho preserved during alpine subduction and collision. In this case, if the scheme of a progressive serpentinization with depth during oceanization is accepted, the successive episodes of serpentinization and deformation could affect this zone preferentially (Fig. 14). This zone constitutes a less competent level, where rheological behaviour of the rock is similar to serpentinite and where the deformation is localized during subduction and exhumation. Thus, during the subduction and then exhumation, the alpine deformation will focus the later steps of serpentinization in this zone and obliterate the gradient of serpentinization.

ACKNOWLEDGEMENTS

F. Boudier is thanked for sharing her knowledge on the Lanzo massif. We thank G. Fabbro and K. Koga (Magmas et Volcans, Clermont Ferrand) for their corrections of the English in this paper. We acknowledge C.

Constantin (Magmas et Volcans, Clermont Ferrand) for thin-section preparation, G. Montagnac (ENS, Lyon) for Raman analyses, J.-L. Devidal (Magmas et Volcans, Clermont Ferrand) for microprobe analyses and J. E. Martelat (Laboratoire de Géologie de Lyon, Lyon) for field work assistance. We thank C. Groppo for critical comments on earlier version of this article, and careful editorial handling by D. Robinson.

REFERENCES

Agrinier, P. & Cannat, M., 1997. Oxygen isotopic constraints on serpentinization processes in ultramafic rocks from the Mid-Atlantic Ridge (23°N) in the MARK area. In: *Proceedings of the Ocean Drilling Program, Scientific Results* (eds Karson, J.A., Cannat, M., Miller, D.J. & Elthon, D.), **153,** 381–388.

Andreani, M., Mével, C., Boullier, A.-M. & Escartin, J., 2007. Dynamic control on serpentine crystallization in veins: constraints on hydration processes in oceanic peridotites. *Geochemistry, Geophysics, Geosystems*, **8,** Q02012, doi: 10.1029/2006GC001373.

Angiboust, S., Langdon, R., Agard, P., Waters, D. & Chopin, C., 2011. Eclogitization of the Monviso ophiolite (W. Alps) and implications on subduction dynamics. *Journal of Metamorphic Geology*, **30,** 37–61.

Auzende, A.-L., Daniel, I., Reynard, B., Lemaire, C. & Guyot, F., 2004. High-pressure behavior of serpentine minerals: a Raman spectroscopic study. *Physics and Chemistry of Minerals*, **31,** 269–277.

Auzende, A.L., Guillot, S., Devouard, B. & Baronnet, A., 2006. Serpentinites in Alpine convergent setting: effects of metamorphic grade and deformation on microstructures. *European Journal of Mineralogy*, **18,** 21–33.

Bach, W., Garrido, C.J., Paulick, H., Harvey, J. & Rosner, M., 2004. Seawater-peridotite interactions: first insights from ODP Leg 209, MAR 15N. *Geochemistry, Geophysics, Geosystems*, **5,** Q09F26, doi: 10.1029/2004GC000744.

Beltrando, M., Lister, G., Rosenbaum, G., Richards, S. & Forster, M., 2010. Recognizing episodic lithospheric thinning along a convergent plate margin: the example of the Early Oligocene Alps. *Earth Science Reviews*, **103,** 81–98.

Bodinier, J.-L., 1988. Geochemistry and petrogenesis of the Lanzo peridotite body, Western Alps. *Tectonophysics*, **149,** 67–88.

Bodinier, J.-L., Guiraud, M., Dupuy, C. & Dostal, J., 1986. Geochemistry of basic dikes in the Lanzo massif (western alps): petrogenetic and geodynamic implications. *Tectonophysics*, **128,** 75–95.

Boudier, F., 1971. Minéraux serpentineux extraits de péridotites serpentinisées des Alpes Occidentales. *Contributions to Mineralogy and Petrology*, **33,** 331–345.

Boudier, F., 1978. Structure and petrology of the Lanzo peridotite massif (Piedmont Alps). *Geological Society of America Bulletin*, **89,** 1574–1591.

Bromiley, G.D. & Pawley, A.R., 2003. The stability of antigorite in the systems MgO-SiO_2-H_2O (MSH) and MgO-Al_2O_3-SiO_2-H_2O (MASH): the effects of Al^{3+} substitution on high-pressure stability. *American Mineralogist*, **88,** 99–108.

Canales, J.P., Collins, J.A., Escartin, J. & Detrick, R.S., 2000. Seismic structure across the rift valley of the Mid-Atlantic ridge at 23°20′N (MARK area): implications for crustal accretion processes at slow-spreading ridges. *Journal of Geophysical Research*, **105,** 28411–28425.

Cannat, M., Mével, C., Maïa, M. *et al.*, 1995. Thin crust, ultramafic exposure and rugged faulting patterns at the Mid-Atlantic Ridge (22°–24°N). *Geology*, **23,** 49–52.

Chernak, L.J. & Hirth, G., 2010. Deformation of antigorite serpentinite at high temperature and pressure. *Earth and Planetary Science Letters*, **296,** 23–33.

Coogan, L.A., Wilson, R.N., Gillis, K.M. & MacLeod, C.J., 2001. Near-solidus evolution of oceanic gabbros: insights from amphibole geochemistry. *Geochimica et Cosmochimica Acta*, **65,** 4339–4357.

Deschamps, F., Guillot, S., Godard, M., Andreani, M. & Hattori, K., 2011. Serpentinites act as sponges for fluid-mobile elements in abyssal and subduction zone environments. *Terra Nova*, **23,** 171–178.

Dick, H.J.B., Lin, J. & Schouten., H., 2003. An ultraslow – spreading class of ocean ridge. *Nature*, **426,** 405–412.

Drouin, M., Godard, M., Ildefonse, B., Bruguier, O. & Garrido, C.J., 2009. Geochemical and petrographic evidence for magmatic impregnation in the oceanic lithosphere at Atlantis Massif, Mid-Atlantic Ridge (IODP Hole U1309D, 30°N). *Chemical Geology*, **264,** 71–88.

Dungan, M.A., 1979. A microprobe study of antigorite and some serpentines pseudomorphs. *Canadian Mineralogist*, **17,** 771–784.

Ellis, D.J. & Green, D.H., 1979. An experimental study of the effect of Ca upon garnet-clinopyroxene Fe-Mg exchange equilibria. *Contributions to Mineralogy and Petrology*, **71,** 13–22.

Ernst, W.G. & Liu, J., 1998. Experimental phase-equilibrium study of Al- and Ticontents of calcic amphibole in MORB – A semiquantitative thermobarometer. *American Mineralogist*, **83,** 952–969.

Escartin, J., Hirth, G. & Evans, B., 2001. Strength of slighty serpentinized peridotites: implications for the tectonics of oceanic lithosphere. *Geology*, **29,** 1023–1026.

Evans, B.W., 2004. The serpentinite multisystem revisited: chrysotile is metastable. *International Geology Review*, **46,** 479–506.

Fumagalli, P. & Poli, S., 2005. Experimentally determined phase relations in hydrous peridotites to 6.5 GPa and their consequences on the dynamics of subduction zones. *Journal of Petrology*, **46,** 555–578.

Garrido, C.J., Lopez Sanchez-Vizcaino, V., Gomez-Pugnaire, M.T. *et al.*, 2006. Enrichment of HFSE in chlorite-harzburgite produced by high-pressure dehydration of antigorite-serpentinite: implications for subduction magmatism. *Geochemistry, Geophysics, Geosystems*, **6,** 1. doi: 10.1029/2004GC000791.

Groppo, C. & Compagnoni, C., 2007. Metamorphic veins from the serpentinites of the Piemonte Zone, western Alps, Italy: a review. *Periodico di Mineralogica*, **76,** 127–153.

Groppo, C., Rinaudo, C., Cairo, S., Gastaldi, D. & Compagnoni, R., 2006. Micro-Raman spectroscopy for a quick and reliable identification of serpentine minerals from ultramafics. *European Journal of Mineralogy*, **18,** 319–329.

Guillot, S., Schwartz, S., Hattori, K., Auzende, A. & Lardeaux, J.M., 2004. The Monviso ophiolitic Massif (Western Alps), a section through a serpentinite subduction channel. Evolution of the western Alps: insights from metamorphism, structural geology, tectonics and geochronology. *The Virtual Explorer*, **16,** Paper 6.

Hermann, J., Muntener, O. & Scambelluri, M., 2000. The importance of serpentinite mylonite for subduction and exhumation of oceanic crust. *Tectonophysics*, **327,** 225–238.

Holland, T.J.B., 1983. The experimental determination of activities in disordered and short-range ordered jadeite, clinopyroxenes. *Contributions to Mineralogy and Petrology*, **82,** 214–220.

Kaczmarek, M.-A. & Muntener, O., 2008. Juxtaposition of melt impregnation and high temperature shear zone in the upper mantle; Field and petrological constraints from the Lanzo peridotite (Northern Italy). *Journal of Petrology*, **49,** 2187–2220.

Kaczmarek, M.-A. & Muntener, O., 2010. The variability of peridotite composition across a mantle shear zone (Lanzo

massif, Italy): interplay of melt focusing and deformation. *Contributions to Mineralogy and Petrology*, **160,** 663–679.
Keppler, H. & Bolfan-Casanova, N., 2006. Thermodynamics of Water Solubility and Partitioning. *Reviews in Mineralogy and Geochemistry*, **62,** 193–230.
Lagabrielle, Y. & Cannat, M., 1990. Alpine Jurassic ophiolites resemble to the modern central Atlantic basement. *Geology*, **18,** 319–322.
Lagabrielle, Y., Fudural, S. & Kienast, J.R., 1989. La couverture océanique des ultrabasites de Lanzo (Alpes occidentales): arguments lithostratigraphiques et pétrologiques. *Geodinamica Acta*, **3,** 43–55.
Martin, B. & Fyfe, W.S., 1970. Some experimental and theoretical observations on the kinetics of hydratation reactions with particular reference to serpentinisation. *Chemical Geology*, **6,** 185–202.
Matsyuk, S.S. & Langer, K., 2004. Hydroxyl in olivines from mantle xenoliths in kimberlites of the Siberian platform. *Contributions to Mineralogy and Petrology*, **147,** 413–437.
Mellini, M., 1982. The crystal structure of lizardite 1T: hydrogen bonds and polytipism. *American Mineralogist*, **67,** 587–598.
Messiga, B. & Tribuzio, R., 1991. The reaction between olivine and plagioclase as a concequence of fluid-rock interactions during sub-seafloor metamorphism (Al-Mg-gabbros, Northern Apennine ophiolites, Italy). *Schweizerische Mineralogische und Petrographische Mitteilungen*, **71,** 405–414.
Mével, C., 2003. Serpentinization of abyssal peridotites at mid-ocean ridges. *Comptes Rendus Geosciences*, **335,** 825–852.
Mosenfelder, J.L., Deligne, N.I., Asimow, P.D. & Rossman, G.R., 2005. Hydrogen incorporation in olivine from 2-12 GPa. *American Mineralogist*, **91,** 285–294.
Muntener, O., Pettke, T., Desmurs, L., Meier, M. & Schaltegger, U., 2004. Refertilisation of mantle peridotite in embryonic ocean basins: trace element and Nd isotopic evidence and implications for crust mantle relationships. *Earth and Planetary Science Letters*, **221,** 293–308.
Müntener, O., Piccardo, G.B., Polino, R. & Zanetti, A., 2005. Revisiting the Lanzo peridotite (NW-Italy): ''asthenospherization'' of ancient mantle lithosphere. *Ofioliti*, **30,** 111–124.
Nicolas, A., Bouchez, J.L. & Boudier, F., 1972. Interprétation cinématique des déformations plastiques dans le massif de lherzolite de Lanzo (*Alpes piemontaises*) – comparaison avec d'autres massifs. *Tectonophysics*, **14,** 143–171.
Nozaka, T., 2003. Compositional heterogeneity of olivine in thermally metamorphosed serpentinite from Southwest Japan. *American Mineralogist*, **88,** 1377–1384.
Nozaka, T., 2010. A note on compositional variation of olivine and pyroxene in thermally metamorphosed ultramafic complexes from SW Japan. *Okayama University Earth Science Reports*, **17,** 1–5.
Padron-Navarta, J.A., Lopez Sanchez-Vizcaino, V., Garrido, C.J. *et al*., 2008. Highly ordered antigorite from Cerro del Almirez HP–HT serpentinites, SE Spain. *Contributions to Mineralogy and Petrology*, **156,** 679–688.
Pelletier, L. & Müntener, O., 2006. High-pressure metamorphism of the Lanzo peridotite and its oceanic cover, and some consequences for the Sezia-Lanzo zone (northwestern Italian Alps). *Lithos*, **90,** 111–130.
Piccardo, G.B., Zanetti, A., Pruzzo, A. & Padovano, M., 2007. The North Lanzo peridotite body (NW Italy): lithospheric mantle percolated by MORB and alkaline melts. *Periodico di Mineralogia*, **76,** 199–221.
Powell, R., 1985. Regression diagnostics and robust regression in geothermometer/geobarometer calibration: the garnet-clinopyroxene geothermometer revised. *Journal of Metamorphic Geology*, **3,** 231–243.
Prietto, A.C., Dubessy, J. & Cathelineau, M., 1991. Structure-composition relationships in trioctahedral chlorites: a vibrational spectroscopy study. *Clays and Clay Minerals*, **39,** 531–539.
Rinaudo, C., Gastaldi, D. & Belluso, E., 2003. Characterization of chrysotile, antigorite, and lizardite by FT-Raman spectroscopy. *Canadian Journal of Mineralogy*, **41,** 883–890.
Rubatto, D., Muntener, O., Barnhoorn, A. & Gregory, C., 2008. Dissolution-reprecipitation of zircon at low-temperature, high-pressure conditions (Lanzo Massif, Italy). *American Mineralogist*, **93,** 1519–1529.
Ryburn, R.J., Raheim, A. & Green, D.H., 1975. Determination of the P, T paths of natural eclogites during metamorphism-record of subduction. *Lithos*, **9,** 161–164.
Scambelluri, M., Hoogerduijn Strating, E.H., Piccardo, G. B., Vissers, R.L.M. & Rampone, E., 1991. Alpine olivine- and titanian clinohumite-bearing assemblages in the Erro-Tobbio peridotite (Voltri Massif, NW Italy). *Journal of Meramorphic Geology*, **9,** 79–91.
Scambelluri, M., Muntener, O., Hermann, J., Piccardo, G.B. & Trommsdorff, V., 1995. Subduction of water into the mantle: history of an Alpine peridotite. *Geology*, **23,** 459–462.
Schwartz, S., Allemand, P. & Guillot, S., 2001. Numerical model of the effect of serpentinites on the exhumation of eclogitic rocks: insights from the Monviso ophiolitic massif (Western Alps). *Tectonophysics*, **342,** 193–206.
Trommsdorff, V., Lopez Sanchez-Vizcaıno, V., Gomez-Pugnaire, M.T. & Muntener, O., 1998. High pressure breakdown of antigorite to spinifex-textured olivine and orthopyroxene, SE Spain. *Contributions to Mineralogy and Petrology*, **132,** 139–148.
Ulmer, P. & Trommsdorff, V., 1995. Serpentinite stability to mantle depths and subduction related magmatism. *Science*, **268,** 858–861.
Vitale-Brovarone, A., Beltrando, M., Malavieille, J. *et al*., 2011. Inherited Ocean-Continent Transition zones in deeply subducted terranes: insights from Alpine Corsica. *Lithos*, **124,** 273–290.
Viti, C. & Mellini, M., 1998. Mesh textures and bastites in the Elba retrograde serpentinites. *European Journal Mineralogy*, **10,** 1341–1359.
Whitney, D.L. & Evans, B.W., 2010. Abbreviations for names of rock-forming minerals. *American mineralogist*, **95,** 185–187.
Wicks, F.J. & Whittaker, E.J.W., 1977. Serpentine texture and serpentinisation. *Canadian Mineralogist*, **15,** 459–488.
Wunder, B. & Schreyer, W., 1997. Antigorite: high-pressure stability in the system MgO-SiO,-H,O (MSH). *Lithos*, **41,** 213–227.
Zhao, Y.H., Ginsberg, S.B. & Kohlstedt, D.L., 2004. Solubility of hydrogen in olivine: dependence on temperature and iron content. *Contributions to Mineralogy and Petrology*, **147,** 155–161.

Received 22 November 2011; revision accepted 13 September 2012.